Research Square

Preprints are preliminary reports that have not undergone peer review.
They should not be considered conclusive, used to inform clinical practice,
or referenced by the media as validated information.

Perinatal Maternal Microbiome Perturbation Alters Metabolite Signaling and Microglial Responses in a Female Mouse model of Aβ amyloidosis

Piyali Saha
University of Chicago
Nicholas Slimmon
The University of Texas Southwestern Medical Center
Ananya Nadgauda
University of Chicago
Priyam Patel
Northwestern Medicine
Diya Mishra
University of Chicago
Pedro Blauth Poli
University of Chicago
Ana Inukai
University of Chicago
Ahtziri Fernandez
University of Chicago
Ian Weigle
University of Chicago
Xiaoqiong Zhang
University of Chicago
Sangram S. Sisodia
ssisodia@bsd.uchicago.edu
University of Chicago

Research Article

Keywords:

Posted Date: November 18th, 2026

DOI: https://doi.org/10.21203/rs.3.rs-11613626/v1

License: This work is licensed under a Creative Commons Attribution 4.0 International License.
Read Full License

Additional Declarations: No competing interests reported.

Perinatal Maternal Microbiome Perturbation Alters Metabolite Signaling and Microglial Responses in a Female Mouse model of Aβ amyloidosis

Piyali Saha*[1], Nicholas Slimmon[2], Ananya Nadgauda[1], Priyam Patel[3], Diya Mishra[1], Pedro Blauth Poli[1], Ana Inukai[1], Ahtziri Fernandez[1], Ian Weigle[1], Xiaoqiong Zhang[1], Sangram S. Sisodia*[1]

[1]Department of Neurobiology, The University of Chicago, Chicago, IL, USA; [2] School of Biomedical Sciences, UT Southwestern Medical Center, Dallas, Texas, USA; [3]Center for Genetic Medicine, Northwestern University, Chicago, IL, USA

*Correspondence to Sangram S. Sisodia: ssisodia@bsd.uchicago.edu and Piyali Saha: piyali@uchicago.edu

Abstract

Maternal microbiome-dependent programming of neuroimmune and metabolic pathways during early development may critically shape sex-specific susceptibility to Alzheimer's disease (AD) later in life. We have documented that in mouse models of Aβ deposition, broad-spectrum antibiotic (ABX)-mediated perturbations of the gut microbiome postnatally (P14-P21) selectively reduces Aβ pathology only in male, but not in female animals. Here, we shift the developmental window upstream to test whether perinatal maternal microbiome perturbations shapes the pathological trajectories of offspring. Dams were treated with the broad-spectrum ABX from preconception through gestation, without direct exposure of the offspring. Strikingly, maternal microbiome disruption selectively reduced cortical Aβ burden in female offspring, with no effect in males, effectively reversing the sex bias observed following postnatal ABX manipulations. To explore the mechanisms underlying this effect, we now report that female offspring exhibited coordinated shifts in

microbial composition and amino acid metabolism, that are coupled to cortical transcriptional programs enriched for GPCR signaling and Rho GTPase pathways. As many microbial metabolites and amino acid-derived ligands signal through GPCRs that are expressed by microglia, these transcriptional changes suggest enhanced GPCR-mediated nutrient sensing in microglia of female animals. These systems level changes in microglia drive a metabolically engaged amyloid clearing phenotype, providing a mechanistic link between maternal microbiome disruption and enhanced Aβ clearance in females. Our study highlights developmental timing as an important determinant of microbiome-associated changes in microglial phenotypes and amyloid pathology in AD mice.

Introduction

Alzheimer's disease (AD) is characterized by the deposition of amyloid β (Aβ) peptides in extracellular plaques and the accumulation of hyperphosphorylated tau as intracellular neurofibrillary tangles within neurons. These pathological lesions lead to synaptic dysfunction, progressive neurodegeneration, neuronal loss, and ultimately cognitive decline and dementia (Price and Sisodia, 1998). Despite decades of research, there are few effective disease-modifying treatments that can prevent or halt disease progression, and current anti-Aβ therapies that are expensive provide only modest, temporary benefits and have significant side effects(Parums, 2024). Recent research has uncovered a pivotal role of the gut microbiome in modulating brain physiology through the gut–brain axis (Cryan et al., 2019). Dysbiosis has been linked to neurodevelopmental and neurodegenerative disorders, including AD, through immune, metabolic, and endocrine pathways (Bicknell et al., 2023). We have shown that postnatal ABX-induced microbiome dysbiosis reduces Aβ pathology and microglial activation in mouse models of Aβ amyloidosis that occurs specifically in male, but not female animals (Dodiya et al., 2019; Minter et al., 2016). To these efforts, we have

demonstrated that estradiol-mediated elevation of amyloid pathology at later ages is, at least in part, responsible for lack of an effect of ABX on females (Saha et al., 2024). These findings underscore the temporal specificity of gut microbiome perturbation as a confounding factor in sex-dependent microbial–neural interactions. In this study, we therefore sought to investigate how perinatal maternal microbiome perturbations during early development influences microbiome composition, cortical transcriptomes and amyloid pathology in the offspring.

The maternal microbiome plays a foundational role in shaping fetal immune and metabolic programming (Koren et al., 2024). Microbial metabolites and immune mediators cross the placental barrier, influencing neurodevelopmental pathways and establishing life-long trajectories of brain function (Di Gesu et al., 2021; Edwards et al., 2017; Vuong et al., 2020). Perturbations in maternal microbiota during pregnancy have been implicated in disorders with pronounced sex bias, including autism spectrum disorders (ASD) and metabolic syndromes (Biagioli et al., 2025; Salia et al., 2025), suggesting that maternal microbial inheritance may confer differential risk across sexes.

In this study, we hypothesized that disruption of the maternal gut microbiome could alter the microbiome of offspring and by so doing, reprogram the metabolic landscape of microglia and other CNS cell types that could lead to alterations in amyloid pathology. Using the APPPS1-21 transgenic mouse model of Aβ amyloidosis, we treated dams with a broad-spectrum ABX cocktail from preconception through gestation to induce maternal microbiome dysbiosis without directly altering the postnatal microbiota of the offspring. This design allowed us to isolate prenatal microbial effects on fetal brain and immune development. We refer to this approach as maternal microbiome perturbation because the intervention specifically targets the gut microbiota of the dams during the critical window of conception

and pregnancy, thereby influencing fetal development largely through maternal immune, hormonal, and metabolic pathways rather than directly altering the postnatal microbiome of the offspring. In this model, dams were separated on the day of copulation, ensuring that the altered maternal microbiome exerted the predominant influence on fetal development and subsequent disease trajectory.

We implemented an integrative multi-omics approach combining 16S rRNA and shotgun metagenomic sequencing, metabolomics, and cortical transcriptomics, complemented by immunohistochemical analyses of Aβ pathology and microglial phenotypes. Our results reveal that maternal microbiome perturbation induces sex-specific microbial and metabolic remodeling leading to alterations in amino acid metabolism and activation of GPCR-linked nutrient-sensing pathways in female offspring. Our findings establish a mechanistic framework in which maternal microbial perturbation programs female-specific neuroprotection through metabolic reorganization and cortical GPCR activation. This work underscores the developmental timing and sex specificity of microbiome-brain interactions and highlights maternal microbial inheritance as a key determinant of AD vulnerability.

Results

16s rRNA sequencing reveals maternal gut microbiome perturbation leads to changes in microbial diversity in offspring

A schematic representation of the ABX treatment and experimental timeline used to evaluate the impact of maternal microbiome perturbations is shown in Figure 1A. Analysis of cecum weight relative to body weight shows a significant increase in male (MM(ABX)_Male) and female (MM(ABX)_Female) pups born to ABX exposed dams compared with male (MM(Ctrl)_Male) or female (MM(Ctrl)_Female) offspring from water-treated dams (Figure 1S,

left panel). Morphological examination further reveals that the ceca from all ABX-treated pups are enlarged and distended as a result of localized inflammation and fluid retention (Figure 1B, right panel). Taxonomic profiling of cecal bacteria at the phylum level demonstrates a pronounced shift in microbial composition across treatment groups (Figure 1B, a). Interestingly, the microbial communities of male and female pups born to ABX-treated dams exhibit clear sex-specific patterns, with male and female offspring forming distinct clusters. Alpha diversity analysis using the Chao1, Inverse Simpson, and Shannon indices reveals changes in microbial richness and evenness in all offspring from ABX-treated mice compared with offspring from vehicle-treated dams (Figure 1B, b). Offspring from ABX-treated dams also show a reduction in microbial diversity compared with controls, although this reduction is less pronounced than that observed in cecal contents of dams that were treated with ABX. Statistical comparisons indicate a significant difference for the Chao1 index ($p < 0.05$), whereas the Inverse Simpson and Shannon indices do not reach statistical significance. The Chao1 index estimates species richness by approximating the number of distinct taxa present, the Inverse Simpson index emphasizes community dominance and evenness, and the Shannon index integrates both richness and evenness. Together, these metrics suggest that maternal ABX exposure alters microbial diversity and community balance, with sex-dependent differences in the magnitude and pattern of these changes.

Principal coordinates analysis (PCoA) of beta diversity, based on both Unweighted UniFrac and Bray–Curtis dissimilarity metrics, further reveals distinct clustering patterns (Figure 1B, c). PERMANOVA analysis confirms that the overall microbiome composition differs significantly between offspring from ABX-treated and vehicle-treated dams. Notably, male and female offspring segregate into separate clusters, indicating sex-dependent microbial restructuring following maternal microbiome perturbation. Collectively, these findings

demonstrate that maternal ABX exposure differentially shapes the gut microbial landscape of male and female progeny rather than exerting an equivalent effect across sexes.

MaAsLin2 analysis revealed pronounced sex-dependent microbial responses to maternal ABX exposure (Figure 1B,e). (MM(ABX)_Female) animals exhibited a broader and stronger enrichment of several microbial taxa compared with (MM(ABX)_Male) animals, indicating enhanced colonization and restructuring of the gut microbiome. At the family level, *Bacteroidaceae, Akkermansiaceae, Enterococcaceae, Porphyromonadaceae, Rikenellaceae,* and *Sutterellaceae* showed stronger positive associations in (MM(ABX)_Female) pups compared with (MM(ABX)_Male) pups. Similarly, several genera displayed markedly higher enrichment in (MM(ABX)_Female) pups, including *Blautia, Phocaeicola, Akkermansia, Enterococcus, Bacteroides, Prevotella, Parasutterella, Dubosiella,* and *Faecalicoccus*, suggesting an expansion of Bacteroidota- and Verrucomicrobia-associated lineages. In contrast, (MM(ABX)_Male) pups exhibited fewer positively associated taxa and retained a greater proportion of genera typically enriched in (MM(Ctrl)_Male) pups, including *Lactobacillus, Bifidobacterium, Muribaculum, Ruminococcus,* and *Clostridium XlVa*, indicating reduced microbial recolonization following maternal microbiome perturbation. Collectively, these findings demonstrate that maternal ABX exposure induces a more pronounced restructuring and enrichment of specific microbial lineages in female offspring, whereas male offspring display comparatively limited microbiome reconstitution.

Collectively, these findings indicate that female offspring exhibit a stronger microbial response to maternal ABX-induced perturbation, characterized by broader enrichment of multiple taxa and greater restructuring of the gut microbial community. In contrast, male offspring display a comparatively limited taxonomic shift and retain a larger proportion of taxa associated with offspring from vehicle-treated dams, consistent with reduced

recolonization and a more constrained microbiome response following maternal ABX exposure.

Gut Microbiota Perturbation of Dams Reduces Aβ Burden in Female Offspring

Immunofluorescence analysis of cortical Aβ plaque deposition using Aβ-specific 3D6 antibody (Figure 2A) revealed sex-specific effects of gut microbiota perturbations. While Aβ burden remained comparable between (MM(Ctrl)_Male) and (MM(ABX)_Male) animals at the time of sacrifice, a statistically significant reduction in Aβ plaques was observed in (MM(ABX)_Female) relative to their control counterparts from vehicle-treated dams ($p < 0.05$; Figure 2B). These findings suggest that maternal microbiome alterations selectively modulate Aβ accumulation in a sex-dependent manner, with a pronounced effect in females. Western blot analysis of the transgene-encoded full-length amyloid precursor protein 751 isoform (APP-FL) in cortical extracts (Figure 2C) demonstrated no significant differences in APP levels between pups from vehicle- and ABX-treated dams of either sex. Densitometric quantification across both male and female groups revealed that the observed reduction in Aβ burden in (MM(ABX)_Female) pups relative to (MM(Ctrl)_Female) pups is not attributable to altered steady-state levels of APP. We further examined the steady-state levels of BACE1 and PS1, two key enzymatic components of the amyloidogenic APP-processing pathway. Western blot analysis showed no significant differences in levels of BACE1 or PS1 (PS1-NT is the amino-terminal derivative generated by autocatalytic processing of full-length PS1) between control and maternal ABX groups in either male or female offspring (Figure 2D–E). Together, these findings indicate that the female-specific reduction in Aβ pathology following maternal ABX treatment occurs without detectable changes in APP abundance or in the protein levels of these major components of the amyloidogenic APP-processing pathway.

Metagenomic profiling reveals sex-specific alterations in gut microbiota of offspring

The taxonomic composition of the gut microbiota in offspring varied markedly across sex and ABX treatment (Figure 3A). In (MM(Ctrl)_Male) pups, the microbiota was dominated by *Bacteroides acidifaciens*, *Bacteroides caecimuris*, and *Candidatus Arthromitus* sp. SFB_mouse. In (MM(ABX)_Male), we observed a drastic reduction of these taxa, accompanied by increases in *Blautia pseudococcoides*, *Burkholderiaceae bacterium*, and *Phocaeicola sartorii*. In comparison, (MM(Ctrl)_Female) exhibited a more diverse microbiota, characterized by higher relative abundances of *Bacteroidales bacterium*, *Lactobacillus johnsonii*, *Muribaculaceae bacterium isolate 104 HZI*, and *Lactobacillus reuteri*. Moreover, in (MM(ABX)_Female) pups, we observed a marked loss of these latter taxa, with concomitant increases in *Xylanibacter rodentium*, *Parabacteroides distasonis*, and *Phocaeicola sartorii*, indicating a pronounced ABX-driven restructuring of the gut community. Several strains exhibited baseline sex differences in (MM(Ctrl)_Male) and (MM(Ctrl)_Female) pups (Figure 3C), including higher *Bacteroidales bacterium* and *Adlercreutzia sp. DSM 108611* in (MM(Ctrl)_Female) pups and *Adlercreutzia sp. DSM 109821* in (MM(Ctrl)_Male) pups. Both *Adlercreutzia* species were nearly depleted in (MM(ABX)_Female) pups. Notably, *L. johnsonii* and *L. reuteri*, species that are linked to methionine-associated metabolic pathways critical for one-carbon metabolism and methyl-donor balance, were significantly more abundant in (MM(Ctrl)_Female) pups than in (MM(ABX)_Female) pups ($p < 0.005$), and both species were either low or undetectable in males, underscoring their female-specific depletion following maternal microbiome perturbation. A subset of taxa, including *Akkermansia muciniphila*, *Dubosiella newyorkensis*, *Blautia pseudococcoides*, *Burkholderiaceae bacterium*,

Parabacteroides distasonis, and *Phocaeicola sartorii*, increased significantly in both sexes after ABX exposure ($p < 0.05$ to $p < 0.0001$), suggesting sex-independent recolonization. Conversely, *Bifidobacterium pseudolongum*, *Bacterium_1XD21_13*, and *Clostridia bacterium* declined significantly in both sexes ($p < 0.05$ to $p < 0.0001$). ABX-induced maternal microbial perturbation also produced more extensive compositional changes in (MM(ABX)_Female) pups than in (MM(ABX)_Male) pups (Figure 3A). Specifically, *Muribaculum intestinale*, *Clostridium innocuum*, *Clostridium cocleatum*, *Desulfovibrionaceae bacterium*, *Rodentibacter heilii*, and *Bacteroides muris* were markedly reduced in (MM(ABX)_Female) pups ($p < 0.05$ to $p < 0.001$), while *Xylanibacter rodentium* and *Staphylococcus xylosus* showed female-specific increases ($p < 0.05$ to $p < 0.001$). Male-specific differences included elevated *Bacteroides acidifaciens* and *Bacteroides caecimuris* in (MM(Ctrl)_Male) ($p < 0.0001$) and reduced *Turicimonas muris* and *Candidatus Arthromitus* in (MM(ABX)_Male) ($p < 0.05$ to $p < 0.0001$).

Overall, the magnitude and diversity of microbial alterations were greater in females, highlighting their heightened susceptibility of female pups to maternal ABX exposure. Some non-significant trends, including reduced abundance of *Bacterium_1XD42_1*, *Alistipes sp. DSM 112343*, *Alistipes indistinctus*, *Coriobacteriaceae bacterium*, and *Muribaculaceae* isolates, further support sex- and ABX-dependent remodeling of the gut microbial ecosystem. To further evaluate similarities in microbial restructuring across groups, we performed linear regression–based correlation analyses comparing species-level abundances (Figure 3B). A very weak but statistically significant positive correlation was observed between MM(ABX)_Female and MM(ABX)_Male microbiomes ($R^2 = 0.1208$, $p = 0.0208$), indicating limited overlap in taxa that recolonize following maternal ABX exposure. Together, these analyses indicate that maternal ABX exposure drives a unique restructuring of the offspring

gut microbiota, with females exhibiting greater taxonomic divergence and more extensive microbial remodeling.

Metabolomic profiling reveals sex-specific changes in metabolite composition

ABX-mediated maternal microbiome perturbation resulted in significant metabolic alterations, particularly in amino acid (Figure 4A and 4S), short-chain fatty acid (SCFA) (Figure 4S), and bile acid (Figure 4S) metabolism. While many metabolite levels changed in male or female pups from ABX-treated dams compared to pups from vehicle-treated dams, the most significant alterations were observed in the amino acid panel (Figure 4A), where there appears to be a sex-dependent effect on microbial fermentation.

Amino acid profiling revealed that (MM(Ctrl)_Female) animals showed higher overall amino acid abundance under control conditions, which markedly decreased in (MM(ABX)_Female) pups, while (MM(ABX)_Male) animals displayed comparatively minor changes compared with (MM(Ctrl)_Male) animals (Figure 4S). For instance, alanine was significantly reduced in (MM(ABX)_Female) animals compared with (MM(Ctrl)_Female) animals ($p < 0.01$) but remained unchanged between (MM(Ctrl)_Male) and (MM(ABX)_Male) animals. Interestingly, (MM(Ctrl)_Female) animals exhibited a significantly higher alanine concentration than (MM(Ctrl)_Male) animals ($p < 0.05$). Similarly, essential amino acids, including leucine, lysine, methionine, and phenylalanine, as well as branched-chain amino acids (BCAAs) including leucine and isoleucine, followed the same pattern, with a significant decrease in (MM(Ctrl)_Female) but no change in (MM(ABX)_Male) animals. Other amino acids, including pantothenic acid, tryptophol, and niacin, also showed a similar trend.

Cysteine and tyrosine showed a significantly higher increase in (MM(Ctrl)_Female) animals compared with (MM(Ctrl)_Male) animals ($p < 0.01$). Aspartate, PreQ1, and

tryptamine exhibited a significant decrease in (MM(ABX)_Female) animals ($p < 0.05$) compared with (MM(Ctrl)_Female) animals, with no significant change in males from vehicle or ABX-treated dams. Additionally, dopamine and quinine levels were significantly increased in (MM(ABX)_Female) animals ($p < 0.01$), with no detectable differences between males from vehicle or ABX-treated dams.

Functional metagenomic–metabolomic integration (Figure 4B) revealed strong sex-specific correlations between microbial pathways and amino acid metabolites. In (MM(Ctrl)_Female) animals, *Lactobacillus johnsonii* and *Lactobacillus reuteri* were enriched and strongly associated with methionine-related routes, including the S-adenosyl-L-methionine (SAM) salvage I (PWY-6151; $p = 0.00053$) and the L-lysine, L-threonine, and L-methionine biosynthesis II (PWY-724; $p = 0.0021$) pathways. These associations were reduced in (MM(ABX)_Female) animals, indicating disruption of methionine metabolism, methyl-donor balance, and one-carbon cycling. Together, these findings indicate that ABX-mediated maternal microbiome perturbations induces sex-specific microbial and metabolic reorganization, wherein female offspring exhibit amino acid restriction through reduced microbial methionine metabolism and host one-carbon regulation.

Transcriptomic analysis reveals sex-specific transcriptional responses in offspring from ABX-exposed dams

We extracted RNA from the dorsal cerebral cortex of male and female APPPS1-21 transgenic mouse offspring born to dams treated with either vehicle or ABX, and performed RNA sequencing to evaluate cortical transcriptional responses to maternal microbiome perturbations. Principal component analysis (PCA) revealed clear separation of samples by sex along the first two principal components (PC1: 33% variance; PC2: 28% variance), with male

and female samples forming distinct clusters (Fig. 5A,a). Within each sex, maternal ABX exposure further shifted the transcriptional profile, with RNA reads from (MM(ABX)_Female) samples forming a distinct cluster relative to RNA reads from (MM(Ctrl)_Female) samples. Consistent with this pattern, a chord diagram illustrating transcriptomic relationships among groups revealed stronger divergence between (MM(Ctrl)_Female) and (MM(ABX)_female) samples compared with (MM(Ctrl)_Male) versus (MM(ABX)_Male) samples, indicating a larger transcriptional shift in the female cortex following maternal microbiome perturbation (Fig. 5A,b).

Differential expression analysis demonstrated a markedly stronger transcriptional response in females compared with males. (MM(ABX)_Female) exhibited 372 differentially expressed genes (DEGs) compared with (MM(Ctrl)_Female), whereas (MM(ABX)_Male) showed only 81 DEGs compared with (MM(Ctrl)_Male) (FDR-adjusted $p < 0.05$) (Fig. 5A,c). Only six genes overlapped between the two comparisons, indicating that the transcriptional response to maternal microbiome perturbation is largely sex-specific.

Hierarchical clustering analysis further illustrated these differences (Fig. 5A,d). RNA from (MM(ABX)-Female) formed a distinct transcriptional cluster that separated clearly from RNA from (MM(Ctrl)_Female), reflecting coordinated gene expression changes across multiple gene modules. In contrast, RNA from (MM(ABX)_Male) showed comparatively smaller transcriptional shifts and clustered closer to transcripts from (MM(Ctrl)_Male), indicating a more limited cortical response to maternal ABX exposure.

Pathway enrichment analysis highlighted GPCR downstream signaling and the Rho GTPase cycle as the most prominent pathways altered in female offspring following maternal ABX exposure (Fig. 5B). These pathways are central regulators of intracellular signaling and cytoskeletal remodeling. Additional enriched categories included regulation of neuron

projection development, plasma membrane–bounded cell projection morphogenesis, and neurotrophin signaling, indicating coordinated alterations in neuronal structure and connectivity. Multiple synaptic processes were also affected, including modulation of chemical synaptic transmission, presynaptic modulation of synaptic transmission, regulation of vesicle fusion, and regulation of neurotransmitter levels. Behavioral and systems-level processes, such as behavior and locomotory behavior, were also represented among the enriched categories. In contrast, pathway enrichment in males was substantially more limited, consistent with the smaller number of DEGs observed in the male cortex.

Pathway enrichment analysis comparing female ABX-treated offspring to male ABX-treated offspring revealed a distinct set of sex-biased biological processes (Figure 5B,c). The most significantly enriched pathway was histone demethylation (GO:0016577), indicating sex-specific epigenetic regulation in response to maternal microbiome disruption. Additional enrichment of positive regulation of translation (GO:0045727) suggests differential control of protein synthesis between sexes under ABX conditions. Immune-related processes, including antigen processing and presentation (GO:0019882), were also overrepresented, pointing to heightened or altered immune signaling in females relative to males. GPCR-related signaling pathways, including class A rhodopsin-like GPCRs (WP189), were enriched, consistent with sex-dependent modulation of receptor-mediated signaling. Developmental and transport-related pathways, such as embryonic organ development (GO:0048568), organic anion transport (GO:0015711), and cellular response to abiotic stimulus (GO:0071214), further distinguished female from male ABX-treated cortices. Together, these findings indicate that maternal ABX exposure induces sex-specific epigenetic, translational, immune, and GPCR-mediated pathway alterations, with females exhibiting a broader and more coordinated transcriptional response than males under identical microbiome perturbation conditions.

Microglial Remodeling Around Amyloid Plaques in Response to Maternal Microbiome Perturbation

To assess how maternal microbiome perturbation influences Aβ-associated neuroinflammation, Iba1 immunofluorescence staining, three-dimensional (3D) reconstruction, and quantitative morphological analyses were performed in cortical sections from female offspring (Figure 6A). Confocal z-stacks were reconstructed in 3D using Imaris to visualize individual Iba1$^+$ microglia and their spatial relationship with Aβ plaques (Figure 6B). In (MM(Ctrl)_Female) mice, large, dense Aβ plaques were surrounded by compact clusters of Iba1$^+$ microglia exhibiting enlarged somata, shorter processes, and reduced branching, consistent with a less ramified plaque-associated morphology. In contrast, (MM(ABX)_Female) mice displayed smaller Aβ plaques surrounded by microglia with smaller somata, longer processes, and greater process branching, reflecting a more highly ramified morphology. These differences were also evident in the 3D reconstructions of microglia surrounding Aβ plaques.

Quantification revealed a significant reduction in the number of Iba1$^+$ microglia in close proximity to Aβ plaques in (MM(ABX)_Female) compared with (MM(Ctrl)_Female) mice. Quantitative analysis of individual Iba1$^+$ microglia further confirmed these morphological differences, demonstrating a significant decrease in soma area (Figure 6a) and significant increases in total process length (Figure 6b), branch points (Figure 6c), junctions (Figure 6c), and terminal endpoints (Figure 6d) in (MM(ABX)_Female) compared with (MM(Ctrl)_Female) mice. Collectively, these findings demonstrate that the reduction in Aβ pathology following maternal microbiome perturbation is accompanied by reduced microglial accumulation

around plaques and a shift toward a more highly branched and ramified microglial morphology.

To further characterize microglial phenotypes within the plaque microenvironment, we examined Clec7a, a marker associated with the microglial neurodegenerative/disease-associated (MGnD/DAM) state, and P2RY12, a marker associated with homeostatic microglia (Butovsky and Weiner, 2018; Paolicelli et al., 2022). Compared with (MM(Ctrl)_Female) mice, (MM(ABX)_Female) mice exhibited a significant reduction in Clec7a^{+} microglia and a concomitant increase in P2RY12^{+} microglia surrounding Aβ plaques (Figure 6C). These molecular changes, together with the decreased soma area and increased process length, branch points, junctions, and terminal endpoints observed in the morphological analyses, support a shift away from a disease-associated microglial phenotype toward a more homeostatic and highly ramified microglial state following maternal microbiome perturbation. Importantly, this altered microglial phenotype was associated with the reduced Aβ burden observed in (MM(ABX)_Female) mice.

Discussion

In a series of preceding efforts, we demonstrated that postnatal ABX-induced microbiome depletion attenuates Aβ deposition and microglial activation in male, but not female, mouse models of Aβ amyloidosis (Dodiya et al., 2019; Minter et al., 2017; Saha et al., 2024). In view of the established role of the maternal microbiome in shaping fetal immune and metabolic programs (Koren et al., 2024), we have examined the impact of ABX-mediated maternal microbiome perturbations on the microbiome composition of male and female offspring and the effects on metabolic processes that might be associated with alterations in Aβ deposition. Our studies offer several important insights into the role of the maternal microbiome in regulation of cellular and physiological processes that mediate AD-type

pathology and neuroinflammation in a mouse model. First, we demonstrate that maternal ABX exposure induces a more pronounced restructuring and enrichment of specific microbial lineages in female offspring, whereas male offspring display comparatively limited microbiome reconstitution. Second, we show that while Aβ burden remained comparable between male animals from vehicle-treated or ABX-treated dams, we observe a statistically significant reduction in Aβ plaques in female offspring from ABX-treated dams compare with their counterparts from vehicle-treated dams. These findings suggest that maternal microbiome alterations selectively modulate Aβ accumulation in a sex-dependent manner, with a pronounced effect in females. Third, metabolomic profiling of cecal contents from offspring of ABX-treated dams revealed sex-specific changes in metabolite composition, particularly in amino acids, short-chain fatty acids (SCFA), and bile acids (Figure 4S) compared with the levels in ceca from offspring of vehicle-treated dams. Functional metagenomic–metabolomic integration revealed strong sex-specific correlations between selected microbes and amino acid metabolites. In female offspring from vehicle-treated dams, *Lactobacillus johnsonii* and *Lactobacillus reuteri* were enriched and strongly associated with methionine-related metabolism, including the S-adenosyl-L-methionine (SAM) salvage I (PWY-6151; $p = 0.00053$) and the L-lysine, L-threonine, and L-methionine biosynthesis II (PWY-724; $p = 0.0021$) pathways. These associations were reduced in female offspring from ABX-treated dams indicating disruption of methionine metabolism, methyl-donor balance, and one-carbon cycling, pathways that regulate epigenetic remodeling and redox homeostasis (Xing and Tu, 2025; Yan et al., 2025). As epigenetic changes are attributed to methylation of lysine residues on histones, and SAM is a methyl donor, pathway enrichment analysis comparing female and male offspring from ABX-treated dams showed a significant enrichment of histone demethylation (GO:0016577) in females. In this regard, methionine restriction (MR),

385 previously been shown to enhance metabolic flexibility and longevity (Kosakamoto et al.,
386 2023; Latimer et al., 2018; Yan et al., 2025; Zhang et al., 2024), also leads to reduced Aβ
387 accumulation in APP/PS1 mice (Xi et al., 2023).

388 Fourth, our transcriptomic studies of cortical RNAs in male and female offspring from
389 vehicle- or ABX-treated dams and now observe a markedly stronger transcriptional response
390 in females compared with males. Pathway enrichment analysis highlighted GPCR downstream
391 signaling and the Rho GTPase cycle as the most prominent pathways altered in female
392 offspring following maternal ABX exposure. While these pathways are central regulators of
393 intracellular signaling and cytoskeletal remodeling, the impact on specific cortical cell types is
394 uncertain. Finally, Ms4a3, a gene associated with peripheral myeloid lineages, was
395 downregulated in the cortex of female offspring from ABX-treated dams, that is coincident
396 with reduced amyloid burden. Because Ms4a3 expression is most commonly associated with
397 chronic inflammatory states, vascular dysfunction, and heightened peripheral immune
398 signaling (Mattiola et al., 2021), its reduction in female offspring from ABX-treated dams
399 might reflect attenuation of myeloid transcriptional signatures associated with amyloid
400 reduction. In this altered inflammatory context, morphological analyses using Iba1 staining
401 revealed that microglia surrounding Aβ plaques in female offspring born to microbiome-
402 perturbed dams displayed elongated, highly ramified dendritic processes, consistent with a
403 homeostatic state. Consistent with these effects, reduced amyloid burden in offspring from
404 ABX-treated dams was associated with a decreased abundance of Clec7a^{+} degenerative
405 microglia (MGnD/DAM) and a concomitant increase in P2ry12^{+} homeostatic microglia within
406 the immediate plaque microenvironment. Collectively, these findings support a model in
407 which maternal microbiome perturbation induces immune transcriptional reprogramming
408 that biases microglia toward a metabolite-responsive, GPCR-driven activation state that

favors morphological plasticity and efficient Aβ clearance while limiting degenerative microglial phenotypes. This GPCR-linked microglial activation state aligns with the paradigm that microbial metabolites crossing the blood–brain barrier directly modulate microglial and clearance capacity through ligand–receptor signaling (Erny et al., 2015; Young and Samuel, 2025). We propose that maternal microbiome perturbation primes microglia in females toward a GPCR-driven, metabolite-responsive phenotype that facilitates Aβ clearance and maintains neuroimmune equilibrium—analogous to metabolic reprogramming observed under MR conditions (Kosakamoto et al., 2023; Latimer et al., 2018; Yan et al., 2025; Zhang et al., 2024).

It should be noted GO terms in our analyses (Figure 5B-a) such as presynaptic modulation of neurotransmission (GO:0099171), inhibitory postsynaptic regulation (GO:0098828), neurotransmitter homeostasis (GO:0001505), vesicle fusion (GO:0031338), neurotrophin signaling (GO:0038179), and neuronal projection development (GO:0010975) indicate that the enriched pathways are predominantly associated with neuronal physiology and synaptic signaling. This is not unexpected or surprising as developmental processes and organization in the offspring are still ongoing during the period of maternal microbiome dysbiosis and after birth. Indeed, the volcano plots (Figure 5A-e) clearly show an elevation in NT3 (neurotrophin 3), a neurotrophic factor secreted by astrocytes that is known to regulate neuronal survival, differentiation, and synaptic function in both the peripheral and central nervous systems (BARBACID, 1995; Ernfors et al., 1994) and synaptotagmin (Syt17), a multifunctional regulator of intracellular protein trafficking in excitatory hippocampal neurons (Ruhl et al., 2019). We also observe a significant elevation in Kallikrein-related peptidase 12 (KLK12), a member of the serine protease family that is expressed by astrocytes in the human brain. A homologue of KLK12, termed KLK7, is a known Aβ degrading enzyme

(Kidana et al., 2018) and in view of the sequence and structural similarity of the KLKs, it is not inconceivable that KLK12 also shares Aβ-degradative activity, that would explain the reduction in Aβ burden in female offspring of ABX-treated dams. Whether KLK12 is a *bona fide* Aβ degrading enzyme is uncertain but knockout and overexpression studies *in vitro* and *in vivo* would be critical to support, or refute this proposal. We also examined whether the reduction in Aβ pathology could be associated with alterations in the amyloidogenic APP-processing pathway. However, protein levels of APP-FL, BACE1, and PS1-NT were unchanged following maternal ABX treatment in both male and female offspring. These findings suggest that the female-specific reduction in Aβ pathology is unlikely to result from altered APP abundance or processing through the BACE1/PS1-dependent pathway and instead support the possibility that mechanisms affecting Aβ clearance or degradation may contribute to the observed phenotype.

The concept that maternal microbial inheritance imprints long-term neuroimmune trajectories is supported by the seminal work of Garel, Thion and colleagues (Thion et al., 2018), which demonstrated that the maternal microbiota regulates fetal microglial maturation at transcriptomic and chromatin-accessibility levels. Their study revealed sex- and time-specific windows of vulnerability to maternal microbiome absence—males being more affected in utero, while females exhibit greater alterations in adulthood. Multiple studies now demonstrate that female offspring are consistently more vulnerable to maternal perturbations involving the gut microbiome and diet. Maternal diet–microbiome disturbances drive epigenetic and developmental alterations that are more pronounced in females, highlighting their heightened sensitivity to early microbial and nutritional cues (Keleher et al., 2018; Masuyama et al., 2015). Recent work further shows that disruptions to the maternal microbiome produce sex-dependent alterations in brain development of

offspring, with female offspring exhibiting more pronounced structural changes in the prefrontal cortex and distinct shifts in microbial colonization, underscoring a clear female-biased vulnerability (Gohmann et al., 2025). In our previous studies, direct ABX treatment of offspring during P14–P21 produced sex-dependent effects on AD pathology (Dodiya et al., 2018, 2021; Saha et al., 2024), whereas the present study uses maternal ABX treatment and therefore represents a substantially different developmental exposure. Consistent with this concept, Lynch et al. (2023) demonstrated that treatment with the same broad-spectrum ABX cocktail during closely spaced postnatal windows (P2–P9, P12–P18, or P21–P27) produced distinct and even opposing sex-dependent immune responses. P2–P9 treatment increased LY6C−/CX3CR1+ monocytes in adult males but not females, whereas P21–P27 treatment increased this population in females but not males; early P2–P9 treatment also increased microglial soma size selectively in females (Lynch et al., 2023). These findings highlight how relatively small shifts in the developmental timing of microbiome perturbation can produce markedly different sex-dependent neuroimmune outcomes. This is consistent with our finding that female offspring from ABX-treated dams exhibit a distinct postnatal response to maternal microbiome perturbations, marked by microglial metabolic reprogramming and enhanced Aβ clearance.

Although this study provides important insights into how maternal microbiome perturbation shapes sex-dependent neuroimmune and metabolic pathways in AD, there are several limitations. Our broad-spectrum ABX-mediated maternal microbiome perturbation paradigm does not identify the specific taxa or metabolites responsible for the observed effects on offspring. Future studies using targeted microbial manipulations, gnotobiotic models, or metabolite supplementation will be required to define the microbial species and metabolic pathways that drive these neuroimmune changes. In addition, although our multi-

omics analyses suggest a link between microbial metabolic alterations, GPCR signaling, and microglial remodeling, the causal receptor–ligand interactions remain to be experimentally validated. Functional studies using GPCR-specific perturbations, microglia-specific receptor knockouts, or metabolite restoration approaches will be necessary to directly test this signaling axis and determine how maternal microbiome perturbations influence neuroimmune trajectories across development and aging. An additional limitation is that the offspring were examined at 3 months of age. In the APPPS1-21 model, cortical Aβ plaque deposition begins at approximately 6–7 weeks of age and is already robust by 3 months, allowing us to examine the effects of maternal microbiome perturbation at a stage of established amyloid pathology. However, aging is accompanied by substantial changes in microglial phenotype and function, including the emergence of senescence-associated and dysfunctional states. Therefore, the microglial response to maternal microbiome perturbation and its relationship to Aβ pathology may differ in aged animals. Examining later ages will be important for determining whether the female-specific reduction in Aβ pathology and associated microglial phenotype observed at 3 months persist, diminish, or change with aging.

A potential caveat in this study is that while pups were still nursing before weaning, they may have consumed small amounts of ABX-containing water from the maternal drinking bottle, resulting in direct exposure estimated at approximately 1/50th of the gavage dose. Nevertheless, given the substantially lower potential direct exposure, the effects observed in this paradigm are expected to be predominantly driven by maternal microbiome perturbations. Future studies examining different developmental windows and exposing pups directly to this low ABX dose without altering the maternal microbiome will help further distinguish maternal from direct postnatal effects.

Collectively, our findings position the maternal microbiome as a lifelong determinant of the neuroimmune milieu, capable of biasing sex specific trajectories of neurodegenerative risk. By integrating microbiome, metabolomic, and transcriptomic data, our study supports a developmental model in which maternal microbiome perturbation programs female specific neuroprotection through metabolic and GPCR linked reorganization. In female offspring from ABX-treated dams, maternal dysbiosis induces amino acid restriction and one carbon imbalance that engage GPCR mediated nutrient sensing pathways, promoting microglial remodeling and enhanced Aβ clearance (Figure 7), whereas males exhibit relative metabolic stability that limits transcriptional adaptation and fails to alter amyloid burden. Modulating the maternal microbiome or restoring key microbial metabolites either early or later in life may therefore represent a promising avenue for precision medicine aimed at leveraging sex informed metabolic and immune mechanisms to influence neurodegenerative trajectories.

Material and Methods

Animal handling and housing

APPPS1-21 mice, acquired from M. Jucker at the University of Tubingen, Germany, were raised on a C57BL6Cj background (Radde et al., 2006). In this model, cortical Aβ plaque deposition begins at approximately 6–7 weeks of age and becomes robust by 3 months of age. The mice were kept in sterile micro-isolator cages and provided with standard chow ad libitum. All procedures involving animal experimentation were conducted following approved Animal Care and Use Protocols by the Institutional Animal Care and Use Committee at the University of Chicago. We hereby confirm that this study has been reported in accordance with the ARRIVE (Animal Research: Reporting of In Vivo Experiments) guidelines, as outlined at https://arriveguidelines.org.

Antibiotics treatment

Maternal microbiome depletion was performed following the protocol described by Vuong et al. 2018 (Vuong et al., 2020), consisting of an initial short term ABX gavage (ST ABX) followed by long term ABX exposure ($1/50^{th}$ of gavage dose) in drinking water (LT ABX). Beginning on day 28 (D28), both males and females assigned to the ABX cohort received the standard ABX cocktail by oral gavage for microbiome depletion. The cocktail included 4 mg/ml kanamycin (Sigma Aldrich K4000 5g), 0.35 mg/ml gentamicin (Sigma Aldrich G1914 250mg), 8,500 U/ml colistin (Sigma Aldrich C4461 1g), 2.15 mg/ml metronidazole (Sigma Aldrich M1547 25g), and 0.45 mg/ml vancomycin (Sigma Aldrich V2002 1g), prepared fresh in sterile water (Minter et al., 2016).

At 6 weeks of age, ABX treated males were paired with ABX treated females for mating. To prevent any paternal microbial influence during pregnancy, males were removed immediately upon confirmation of copulation (vaginal sperm detection or vaginal plug) and were not used for further experimental procedures. Following mating, dams transitioned to the LT ABX phase, in which the same ABX cocktail was provided in drinking water at 1/50 of the standard gavage dose throughout pregnancy and lactation. This ensured continuous maternal microbiome depletion from preconception through offspring postnatal day 21 (PND21). Control animals were housed identically but received autoclaved drinking water without ABX. Following weaning at PND21, offspring were group housed according to sex and experimental condition.

Pups remained with their ABX treated dams until PND21, receiving developmental exposure to maternal microbiome disruption without any direct ABX administration. After

552 weaning, all offspring were placed on autoclaved drinking water (no ABX) and maintained
553 under standard conditions until 3 months of age.

554 **Necropsy and tissue harvesting**

555 The procedure for harvesting various organs from mice at the time of sacrifice was
556 conducted according to the approved and published Animal Care and Use Protocols of the
557 University of Chicago. On the day of euthanasia, mice were given an intraperitoneal injection
558 containing a mixture of ketamine and xylazine. After confirming deep anesthesia, blood
559 samples were drawn through cardiac puncture using a 25-gauge needle, then stored in EDTA-
560 coated collection tubes (BD Vacutainer; 365974) and placed on ice. Immediately following
561 blood collection, the descending aorta was clamped, and the mice were perfused with
562 physiological cold saline (pH 7.4) for 3 minutes. The brains were then removed from the skulls
563 and divided into two hemispheres: one was postfixed with 4% paraformaldehyde for
564 histological examination, and the other was immediately frozen for transcriptome analysis.
565 The cecum was collected and weighed to assess the efficacy of the ABX treatments. Upon
566 completion of these procedures, plasma was separated by centrifuging at 2,000 rpm for 10
567 minutes at 4°C using a Beckman Coulter centrifuge and stored at −80°C for future use.

568 **Cerebral cortex RNA extraction**

569 Total RNA was extracted from the dorsal cerebral cortex using Trizol reagent, as per
570 the protocol by Dodiya et al., and cleaned with the RNAeasy Micro kit (Qiagen). Quality
571 assessment was done with an Agilent Bioanalyzer. RNA-seq library preparations and
572 sequencing were performed using an Illumina HiSeq4000 at The University of Chicago
573 Genomics Core Facility. The data were collected in FASTQ format for bioinformatic analysis.

574

575

RNA-seq bioinformatics analysis

The quality of DNA reads, provided in FASTQ format, was assessed using FastQC. Adapters were trimmed, and reads that were either of poor quality or aligned to rRNA sequences were filtered using Trimgalore http://www.bioinformatics.babraham.ac.uk/projects/trim_galore/. The cleaned reads were then aligned to the mouse genome (mm10) using STAR. Read counts for each gene were computed using HTSeq-Counts, in conjunction with a gene annotation file for mm10 obtained from Ensembl (http://useast.ensembl.org/index.html). A comprehensive quality control report was assembled using MultiQC. Differential expression was analyzed using DESeq2, with a cut-off for identifying significant differentially expressed genes (DEGs) set at an FDR-adjusted P value of <0.05. Gene Ontology (GO) analysis and identification of DEGs within specific pathways were conducted using Metascape, and the findings were validated using the DAVID and Gorilla online services.

Fecal DNA extraction

Bacterial DNA was extracted from cecal and fecal contents following the method previously described and in accordance with standardized Earth Microbiome Project protocols (www.earthmicrobiome.org/emp-standard-protocols/). In brief, tissues were dissolved in an extraction buffer (50 mg tissue/ml buffer, 50 mM Tris (pH 7.4), 100 mM EDTA (pH 8.0), 400 mM NaCl, 0.5% w/v SDS) containing 0.4 mg/ml of proteinase K. Upon the addition of glass beads with a diameter of 0.1 mm (500 µl/ml buffer, BioSpec Products), microbial cells were lysed using a Mini-Beadbeater-8K Cell Disrupter (BioSpec Products), followed by overnight incubation in a water bath at 55 °C. Total DNA was subsequently extracted using a Phenol:Chloroform:IAA mixture (25:24:1 v/v, pH 8.0, Ambion), following the manufacturer's guidelines. The DNA yield was quantified, and its quality was determined

using a combination of Nanodrop Lite (Thermo Fisher) and Qubit® fluorometer (Invitrogen) assessments.

16S rRNA gene Illumina® MiSeq sequencing

The 16S rRNA gene copy number was quantified from DNA isolated from fecal and cecal contents using quantitative PCR (QPCR). A concentration of 2–5 ng/µl DNA was combined with iQ-SYBR Green PCR Supermix (Bio-Rad), 518F (5'-TCC-TAC-GGG-AGG-CAG-CAG-T-3') and 338R (5'-GGA-CTA-CCA-GGG-TAT-CTA-ATC-CTG-TT-3') primers (2.5 µM), and Q-PCR was carried out on a LightCycler® 480 system (Roche). The reaction conditions were as follows: an initial denaturation at 95 °C for 5 minutes, followed by 35 cycles of 95 °C for 10 seconds, 64 °C for 45 seconds, and 72 °C for 45 seconds, and a final extension at 40 °C for 30 seconds. The 16S rRNA gene copy number was determined by referencing Cp values to a standard curve created from the pCR4-TOPO plasmid containing the 16S rRNA gene amplicon. The copy number was then expressed relative to the specific DNA concentration added per reaction, as determined by a prior assessment using a Qubit® fluorometer (Invitrogen). All reactions were conducted in triplicate and included appropriate negative controls.

Fecal microbiota analysis

We utilized the Quantitative Insights Into Microbial Ecology (QIIME) pipeline and vsearch 8.1 to conduct standard demultiplexing and quality filtering. Unique ASVs were identified utilizing the Deblur method, and taxonomy was assigned through the Greengenes Database (May 2013 release; http://greengenes.lbl.gov). Statistical analyses were carried out in R, relying primarily on the 'vegan' and 'phyloseq' libraries.

Western Blot Analysis

Brain lysates were prepared from APPPS1-21 mice hemibrains using a lysis buffer composed of 50 mM Tris (pH 7.4), 150 mM NaCl, 5 mM EDTA, 0.5% NP-40, 0.5% sodium deoxycholate, 1x protease inhibitor cocktail, 1 mM PMSF, and 1x phosphatase inhibitor cocktail. Post-homogenization and sonication on ice, samples were centrifuged at 10,000 g for 20 minutes at 4°C. The supernatant was then collected as the total protein lysate. Protein concentrations were quantified using BCA analysis. For gel electrophoresis, samples were denatured at 95°C in reducing buffer prior to running on 12% glycine SDS-PAGE or 10-16.5% tricine SDS-PAGE gels, as described in Minter et al., 2016. This was followed by a wet transfer to a 0.2 µm nitrocellulose membrane. The membranes were blocked in 5% non-fat milk in PBS-T for 1 hour at room temperature. Full-length human APP (APP-FL) was detected using the C1/6.1 antibody (BioLegend; 1:1000). BACE1 (Abcam, #108394, 1:3000) and PS1-NT (Biolegend, #823404, 1:1000) were detected using their respective primary antibodies. β-Actin (Santa Cruz Biotechnology, #56459, 1:10000) and GAPDH (Cell Signaling Technology, #D4C6R, 1:10000) were used as loading controls and detected using the corresponding primary antibodies . Following washing, membranes were incubated with the appropriate HRP-conjugated secondary antibodies at a 1:10,000 dilution for 1 h at room temperature. Chemiluminescent signals were detected using Western Lightning® Plus ECL substrate (PerkinElmer) and visualized using the ChemiDoc MP Imaging System (Bio-Rad). Densitometry analysis was performed using ImageJ.

Immunocytochemistry

To assess microglia in the context of Aβ deposits, immunofluorescence staining was performed, following a previously published protocol. Specifically, a complete series of 40-µm-thick brain sections were stained for Aβ (3D6, 1:10,000) [9], while a half series was used for microglia staining with primary antibodies Iba1 (Invitrogen, 1:1000), P2RY12 (Invitrogen, 1:1000) and Clec7a (Invitrogen, 1:100). The procedure began with washing free-floating, level-matched 40-µm sections in dilution media, with a duration of 60 minutes (10 min per wash). Sections were then immersed in serum blocking solution for an hour at ambient temperature, succeeded by overnight incubation with primary antibodies at 4°C. The subsequent day, the sections underwent a 60-minute wash in dilution media (10 min/wash), followed by a one-hour incubation with secondary antibodies at room temperature. Donkey anti-mouse 488 (Invitrogen; 1:500 and donkey anti-rabbit 647 (Invitrogen; 1:500) were employed as secondary antibodies for Aβ and microglia staining, correspondingly. Afterward, sections were washed, mounted on glass slides, and coverslipped using Fluoromount aqueous mounting medium (Sigma-Aldrich; F4680). The images of 3D6+ Aβ plaques were obtained with a 3D Histech Pannoramic MIDI whole-slide scanner and a Zeiss AxioCam MRM CCD camera, handled by personnel from The University of Chicago Integrated Light Microscopy Facility. Microglia Iba1 images were taken utilizing a Leica SP5 3D STED laser-scanning confocal microscope at 40×1.5 oil magnification and Clec7a/P2ry12 images at 63× oil magnification. For visualization of microglial morphology in three dimensions, confocal z-stacks were reconstructed using Imaris (Oxford Instruments). Three-dimensional reconstruction was used to visualize individual Iba1+ microglia and their spatial relationship to Aβ plaques. Quantitative analysis of individual microglial morphology was performed using Fiji/ImageJ. Individual Iba1+ microglia were analyzed for morphological parameters including

soma area, total process length, number of branch points/junctions, and process endpoints. The same image-processing and quantification criteria were applied across experimental groups.

Abeta burden analysis

Evaluation of Aβ burden was conducted in accordance with a previously defined protocol. Briefly, six equidistant sections at 480 µm intervals, ranging from beyond the olfactory bulb to the mid-hippocampal level, were employed for the analysis of 3D6+ amyloid plaques. The Fiji ImageJ software (NIH; ImageJ 1.51n) was used by two independent and blinded observers to determine the Aβ fractionalarea, also known as the amyloid burden. Individual images were processed using the 3D Histech Panoramic viewer software (3DHistech Kft), and subsequently normalized. Automated thresholding, based on histogram entropy, was applied to identify the amyloid plaques. After converting the images into an 8-bit format, a specific threshold number was applied, and this was followed by the use of the "fill holes" and "watershed" algorithms for binary conversion. Finally, the total area encompassed by plaques (i.e., Aβ burden) were computed using the "analyze particles" function. The Aβ burden, represented as the area fraction, was calculated by dividing the total area occupied by plaques by the total area of the cerebral cortex, which was the region of interest.

Statistical analysis

Statistical analyses were carried out using the GraphPad Prism software, version 7.0e. For comparing the α- and β-diversity indices in the 16S rRNA microbiota analysis across multiple groups, the Wilcoxin analysis was utilized. This allowed for the careful comparison of distributions and medians among different groups, and corrections were made for multiple comparisons to ensure the integrity of the results. For other studies, one-way ANOVA

(Analysis of Variance) was employed, unless otherwise specified in the methodology. The one-way ANOVA enabled the examination of differences among means for several groups, and it was followed by post hoc comparisons to identify which specific groups were different from each other. In all the analyses, a statistical P value below 0.05 was considered indicative of significant differences between the groups under comparison. Further details and specifics regarding the statistical methods and findings, including any additional tests or adjustments that were made, can be found in the figure legends accompanying the results.

Declarations

Ethics approval and consent to participate

All animal experiments were performed in accordance with institutional guidelines and were approved by the Institutional Animal Care and Use Committee (IACUC) at the University of Chicago.

Consent for publication

Not applicable.

Availability of data and materials

The datasets generated and/or analyzed during the current study are available from the corresponding author upon reasonable request. Sequencing data will be deposited in an appropriate public repository prior to publication.

Competing interests

The authors declare that they have no competing interests.

Funding

This work was supported by Cure Alzheimer's Fund, The Luminescence Foundation, the Open Philanthropy Project and Good Ventures Foundation, Creative Minds Care Foundation, and the BrightFocus Foundation.

Acknowledgement

We thank the Slide Scanner Image Processing service at the University of Chicago Integrated Light Microscopy Core Facility. We thank Dr. Pieter W. Faber for his assistance with the Bioanalyzer and next-generation sequencing services at the University of Chicago Genomics Core Facility. We also thank Prof. Pamer for providing access to the Duchossois Family Institute facilities at the University of Chicago, including the full-service pipelines in metabolomics (DFI Microbiome Metabolomics Facility) and genomics (Microbiome Metagenomics Facility).These studies were supported by the Cure Alzheimer's Fund (to S.S. Sisodia), the Open Philanthropy Project and Good Ventures Foundation (to S.S. Sisodia), the Luminescence Foundation (to S.S. Sisodia), Creative Minds Care Foundation (to S.S.Sisodia) and the Safadi Program for Excellence in Clinical and Translational Neuroscience Postdoctoral Fellowship (to P. Saha).

Author contributions

P. Saha performed the ABX experiments; analyzed all omics datasets (including gut microbiota and RNA-seq); analyzed immunohistochemistry and western blot data; and performed SP5 laser confocal imaging., and prepared the final figures and manuscript; N. Slimmon assisted with immunohistochemistry using 3D6 antibody; P. Patel performed the bioinformatics analyses and assisted in generating RNA-seq figures; D. Mishra conducted the western blot experiments; A. Nangudga performed microglial staining; I. Weigle assisted with mouse sacrifice; P. P. Blauth carried out brain sectioning; A. Inukai and A. Fernandez performed RNA isolation; X. Zhang maintained and genotyped the mice; S. S. Sisodia developed the microbiota-related hypothesis, co-designed the experimental study, and reviewed and critiqued the manuscript.

Figure Captions

Figure 1. Maternal ABX exposure induces persistent and sex-dependent gut microbiome remodeling. A, Experimental design. Female breeders received short-term antibiotic (ABX) treatment prior to mating followed by continued exposure during gestation. Offspring were weaned at P21 and analyzed at 3 months of age. Fecal samples from dams and offspring were collected for 16s rRNA sequencing. B, Microbiome profiling. a, Relative taxonomic abundance at the indicated taxonomic levels in maternal and offspring microbiota following control or ABX exposure. b, Alpha diversity indices (Chao1 richness, Shannon index, and Inverse Simpson index). c, Unweighted UniFrac principal coordinates analysis (PCoA) showing phylogenetic β-diversity. d, Bray-Curtis PCoA showing compositional β-diversity. e, Differentially abundant taxa identified using *MaAsLin2*. Statistical significance for alpha diversity was determined using two-sided Wilcoxon rank-sum tests with false discovery rate (FDR) correction. β-diversity differences were assessed using two-sided PERMANOVA (999 permutations) with FDR correction. Differential abundance was determined using a two-sided linear model with Benjamini–Hochberg FDR correction (FDR < 0.05). Data represent individual biological replicates (n = 6 pups per group). *P < 0.05; **P < 0.01; NS, not significant.

Figure 2. Maternal antibiotic exposure alters cerebral cortical amyloid burden in a sex-dependent manner. A, Representative images of 3D6-immunolabeled amyloid plaques in the cerebral cortex of male and female offspring derived from control (MM(Ctrl)) and antibiotic-exposed (MM(ABX)) dams. B, Quantification of cerebral cortical amyloid-β burden across groups. Statistical analysis was performed using one-way ANOVA followed by multiple-comparison correction. C–E, Western blot analysis and densitometric quantification of (C) full-length amyloid precursor protein (APP-FL), (D) β-site amyloid precursor protein cleaving enzyme 1 (BACE1), and (E) presenilin-1 N-terminal fragment (PS1-NT) in the cerebral cortex of

male and female offspring. APP-FL and PS1-NT protein levels were normalized to β-actin, and BACE1 protein levels were normalized to GAPDH. Western blot comparisons were performed using two-sided Student's *t*-tests. Data are presented as mean ± s.e.m.; each point represents an independent biological replicate (immunohistochemistry: $n = 6–9$ per group; western blot: $n = 3$ per group). Scale bar, 50 μm. $P < 0.05$; NS, not significant.

Figure 3. Maternal antibiotic exposure alters species-level microbial composition and intergroup correlations. a, Shotgun metagenomics analysis showing species-level distribution across MM(Ctrl)_Male, MM(ABX)_Male, MM(Ctrl)_Female and MM(ABX)_Female groups (n = 6 mice per group). Pie charts represent relative abundance of dominant bacterial species identified by metagenomic sequencing. b, Linear regression–based correlation analysis comparing relative species abundance between MM(ABX)_Female and the indicated groups. Correlation strength was assessed using two-sided linear regression analysis; the coefficient of determination (R^2) and corresponding P values are shown. Each point represents one bacterial species (n = 44 total species tested; species with missing or zero values in either group were excluded from regression). Statistical significance was defined as $P < 0.05$.

Figure 4. Maternal antibiotic exposure alters metabolite profiles and microbial functional pathways in a sex-dependent manner. a, Targeted metabolomics analysis showing relative abundance of the indicated metabolites in Male_Vehicle, Male_ABX, Female_Vehicle and Female_ABX groups (n = 6 mice per group; total n = 24). Bars represent mean relative abundance across biological replicates. b, Functional metagenomics analysis showing pathway abundance associated with *Lactobacillus johnsonii* (PWY-6151: S-adenosyl-L-methionine salvage I) and *Limosilactobacillus reuteri* (PWY-724: superpathway of L-lysine, L-threonine and L-methionine biosynthesis. Relative abundance of *Lactobacillus johnsonii* (c) and *Lactobacillus reuteri* (d) across groups (n = 6 mice per group; total n = 24). Statistical significance was

792 determined using two-sided Kruskal–Wallis tests followed by multiple-comparison correction.
793 Data are presented as mean ± s.e.m., and each point represents one independent biological
794 replicate. *P < 0.05; **P < 0.01.

795 **Figure 5**. Maternal antibiotic exposure induces sex-specific transcriptional remodeling in the
796 cerebral cortex. A, Cortical RNA transcriptomic analysis of male and female offspring. Principal
797 component analysis (PCA) of variance-stabilized normalized transcript counts demonstrates
798 separation among MM(Ctrl)_Male, MM(ABX)_Male, MM(Ctrl)_Female, and
799 MM(ABX)_Female groups; PC1 and PC2 explain 33% and 28% of the total variance,
800 respectively. Differential gene expression was identified using DESeq2 with a two-sided Wald
801 test for both up- and downregulated transcripts, followed by Benjamini–Hochberg false
802 discovery rate (FDR) correction (FDR < 0.05). The overlap of significantly differentially
803 expressed genes between Female_Ctrl versus Female_ABX and Male_Ctrl versus Male_ABX
804 comparisons is shown. A heatmap of differentially expressed genes with hierarchical
805 clustering was generated using Euclidean distance and complete linkage on scaled expression
806 values. B, Pathway enrichment analysis of differentially expressed genes was performed using
807 Gene Ontology (GO) and Reactome databases with a two-sided hypergeometric test against a
808 whole-genome background, followed by multiple-hypothesis testing with FDR correction (FDR
809 < 0.05). Enriched pathways are ranked by –log10(P). Data represent n = 6 mice per group.
810 Statistical significance was defined as FDR < 0.05.

811 **Figure 6**. Maternal antibiotic exposure alters microglial plaque association and phenotype in
812 the female cortex. A, Representative confocal images of DAPI (blue), 3D6-immunolabeled
813 amyloid plaques (green), and Iba1$^+$ microglia (red) in the cerebral cortex of MM(Ctrl)_Female
814 and MM(ABX)_Female mice. Merged images show Iba1$^+$ microglia in close proximity to 3D6$^+$
815 amyloid plaques. Quantification of Iba1$^+$ microglial somata in close proximity to 3D6$^+$ plaques

816 is shown at right. B, Representative Imaris 3D reconstructions of plaque-localized microglia in
817 the cerebral cortex of MM(Ctrl)_Female and MM(ABX)_Female mice. Quantification of
818 microglial morphological parameters, including (a) cell body area, (b) total dendritic length,
819 (c) number of dendritic branches, (d) number of junctions, and (e) number of terminal points,
820 is shown at right. C, Representative confocal images of 3D6-immunolabeled amyloid plaques
821 (green), Clec7a$^+$ microglia (yellow), and P2ry12$^+$ microglia (red) in the cerebral cortex of
822 MM(Ctrl)_Female and MM(ABX)_Female mice. Merged images show Clec7a$^+$ and P2ry12$^+$
823 microglia in close proximity to 3D6$^+$ amyloid plaques. Quantification of P2ry12$^+$ and Clec7a$^+$
824 microglia in close proximity to 3D6$^+$ plaques is shown at right. Statistical comparisons were
825 performed using two-sided unpaired tests. Each point represents an independent biological
826 replicate. Data are presented as mean ± s.e.m. Scale bars, 20 μm (A, C) and 5 μm (B). **P <
827 0.01; ****P < 0.0001.
828 **Figure 7.** Proposed model linking maternal microbiome disruption to sex-specific cortical
829 remodeling and amyloid-associated microglial responses. Maternal antibiotic exposure alters
830 gut microbial composition, leading to changes in microbial-derived metabolites and functional
831 pathways. These circulating metabolites influence host signaling networks, including growth
832 factor and neurotransmitter pathways, and modulate blood–brain communication. In female
833 offspring, altered metabolic signaling reshapes cortical transcriptional programs and
834 microglial phenotype, influencing plaque-associated microglial responses and amyloid
835 burden. This model integrates metagenomic, metabolomic and transcriptomic findings to
836 propose a gut–metabolite–brain axis mediating sex-dependent effects on neuroinflammatory
837 and synaptic regulation pathways.
838
839

Legends of Supplementary Figures

Figure 1S. Maternal ABX exposure is associated with persistent cecal enlargement in offspring. A, Cecum weight normalized to body weight in male and female offspring derived from control dams [MM(Ctrl)] or antibiotic-treated dams [MM(ABX)] at the experimental endpoint. Offspring from ABX-treated dams exhibited significantly increased cecum weight/body weight ratios in both sexes relative to corresponding controls, consistent with sustained alterations in gut microbial colonization. B, Representative gross images of ceca from each experimental group. a, MM(Ctrl)_Male. b, MM(ABX)_Male. c, MM(Ctrl)_Female. d, MM(ABX)_Female. Enlarged ceca are evident in offspring from ABX-treated dams compared with controls. Statistical significance was determined using one-way ANOVA with appropriate multiple-comparisons testing. Data represent individual biological replicates with mean ± SEM. ****P < 0.0001.

Figure 2S. Full Western blots for APP-FL, BACE1, and PS1-NT in male and female offspring following maternal microbiome perturbation. Full, uncropped Western blot images corresponding to the protein analyses presented in Figure 2 are shown for male and female offspring from control dams [MM(Ctrl)] and antibiotic-treated dams [MM(ABX)]. BACE1 blots and the corresponding GAPDH loading controls are shown on page 1; PS1-NT blots with the corresponding β-actin loading controls are shown on page 2; and APP full-length (APP-FL) blots with the corresponding β-actin loading controls are shown on page 3. Molecular weight markers (kDa) are indicated alongside the blots. For the APP-FL blots, the molecular weight ladder was run on the same gel but is not visible in the displayed blot image because the ladder lane was outside the cropped region containing the sample lanes. The corresponding molecular weight positions are therefore indicated alongside the APP-FL blots based on the original gel. Figure 2S

Figure 4S. Maternal ABX exposure alters cecal metabolite profiles in offspring in a sex-dependent manner. Targeted metabolomic analysis of cecal contents collected from male and female offspring born to vehicle-treated or antibiotic-treated dams at the experimental endpoint revealed changes in representative microbiome-associated metabolites, including amino acids and related compounds such as methionine, alanine, leucine, lysine, phenylalanine, isoleucine, aspartate, cysteine, threonine, glutamine, and asparagine, as well as bile acid derivatives including benzoate, 7-12-dioxolithocholic acid, gamma-muricholic acid, lithocholic acid-3-sulfate, 7-oxodeoxycholic acid, glycolithocholic acid-3-sulfate, cholenic acid, and 12-oxochenodeoxycholic acid. Maternal ABX exposure induced broad and sex-specific remodeling of the offspring cecal metabolome, with particularly prominent alterations in Female_ABX animals, consistent with persistent microbiome-dependent metabolic reprogramming. Statistical significance was determined using one-way ANOVA with appropriate multiple-comparisons testing. Data represent individual biological replicates with mean ± SEM. *P < 0.05; **P < 0.01; ***P < 0.001; ****P < 0.0001.

References

BARBACID, M. 1995. Structural and Functional Properties of the TRK Family of Neurotrophin Receptors. *Annals of the New York Academy of Sciences* 766:442–458.

Biagioli, V., M. Matera, L.A. Ramenghi, R. Falsaperla, and P. Striano. 2025. Microbiome and Pregnancy Dysbiosis: A Narrative Review on Offspring Health. *Nutrients* 17:

Bicknell, B., A. Liebert, T. Borody, G. Herkes, C. McLachlan, and H. Kiat. 2023. Neurodegenerative and Neurodevelopmental Diseases and the Gut-Brain Axis:

887 The Potential of Therapeutic Targeting of the Microbiome. *International Journal of*
888 *Molecular Sciences* 24:9577.
889 Butovsky, O., and H.L. Weiner. 2018. Microglial signatures and their role in health and
890 disease. *Nature Reviews Neuroscience* 19:622–635.
891 Cryan, J.F., K.J. O'Riordan, C.S.M. Cowan, K.V. Sandhu, T.F.S. Bastiaanssen, M. Boehme,
892 M.G. Codagnone, S. Cussotto, C. Fulling, A.V. Golubeva, K.E. Guzzetta, M. Jaggar,
893 C.M. Long-Smith, J.M. Lyte, J.A. Martin, A. Molinero-Perez, G. Moloney, E. Morelli,
894 E. Morillas, R. O'Connor, J.S. Cruz-Pereira, V.L. Peterson, K. Rea, N.L. Ritz, E.
895 Sherwin, S. Spichak, E.M. Teichman, M. van de Wouw, A.P. Ventura-Silva, S.E.
896 Wallace-Fitzsimons, N. Hyland, G. Clarke, and T.G. Dinan. 2019. The Microbiota-
897 Gut-Brain Axis. *Physiol Rev* 99:1877–2013.
898 Di Gesu, C.M., L.M. Matz, and S.A. Buffington. 2021. Diet-induced dysbiosis of the
899 maternal gut microbiome in early life programming of neurodevelopmental
900 disorders. *Neurosci Res* 168:3–19.
901 Dodiya, H.B., T. Kuntz, S.M. Shaik, C. Baufeld, J. Leibowitz, X. Zhang, N. Gottel, X. Zhang,
902 O. Butovsky, J.A. Gilbert, and S.S. Sisodia. 2019. Sex-specific effects of
903 microbiome perturbations on cerebral Abeta amyloidosis and microglia
904 phenotypes. *J Exp Med* 216:1542–1560.
905 Edwards, S.M., S.A. Cunningham, A.L. Dunlop, and E.J. Corwin. 2017. The Maternal Gut
906 Microbiome During Pregnancy. *MCN Am J Matern Child Nurs* 42:310–317.
907 Ernfors, P., K.-F. Lee, and R. Jaenisch. 1994. Mice lacking brain-derived neurotrophic
908 factor develop with sensory deficits. *Nature* 368:147–150.
909 Erny, D., A.L. Hrabe de Angelis, D. Jaitin, P. Wieghofer, O. Staszewski, E. David, H. Keren-
910 Shaul, T. Mahlakoiv, K. Jakobshagen, T. Buch, V. Schwierzeck, O. Utermohlen, E.

911 Chun, W.S. Garrett, K.D. McCoy, A. Diefenbach, P. Staeheli, B. Stecher, I. Amit,
912 and M. Prinz. 2015. Host microbiota constantly control maturation and function
913 of microglia in the CNS. *Nat Neurosci* 18:965–977.
914 Gohmann, L., J.A. Cusick, G.E. Demas, and C.L. Wellman. 2025. Maternal Stress and
915 Maternal Microbiome Manipulations Remodel Offspring Medial Prefrontal Cortex
916 in a Sex-Dependent Manner. *Dev Neurobiol* 85:e22971.
917 Keleher, M.R., R. Zaidi, S. Shah, M.E. Oakley, C. Pavlatos, S. El Idrissi, X. Xing, D. Li, T.
918 Wang, and J.M. Cheverud. 2018. Maternal high-fat diet associated with altered
919 gene expression, DNA methylation, and obesity risk in mouse offspring. *PLoS*
920 *One* 13:e0192606.
921 Kidana, K., T. Tatebe, K. Ito, N. Hara, A. Kakita, T. Saito, S. Takatori, Y. Ouchi, T. Ikeuchi,
922 M. Makino, T.C. Saido, M. Akishita, T. Iwatsubo, Y. Hori, and T. Tomita. 2018. Loss
923 of kallikrein-related peptidase 7 exacerbates amyloid pathology in Alzheimer's
924 disease model mice. *EMBO Mol Med* 10:
925 Koren, O., L. Konnikova, P. Brodin, I.U. Mysorekar, and M.C. Collado. 2024. The maternal
926 gut microbiome in pregnancy: implications for the developing immune system.
927 *Nat Rev Gastroenterol Hepatol* 21:35–45.
928 Kosakamoto, H., F. Obata, J. Kuraishi, H. Aikawa, R. Okada, J.N. Johnstone, T. Onuma,
929 M.D.W. Piper, and M. Miura. 2023. Early-adult methionine restriction reduces
930 methionine sulfoxide and extends lifespan in Drosophila. *Nat Commun* 14:7832.
931 Latimer, M.N., K.W. Freij, B.M. Cleveland, and P.R. Biga. 2018. Physiological and
932 Molecular Mechanisms of Methionine Restriction. *Front Endocrinol (Lausanne)*
933 9:217.

934 Lynch, C.M.K., C.S.M. Cowan, T.F.S. Bastiaanssen, G.M. Moloney, N. Theune, M. van de
935 Wouw, E. Florensa Zanuy, A.P. Ventura-Silva, M.G. Codagnone, F. Villalobos-
936 Manríquez, M. Segalla, F. Koc, C. Stanton, P. Ross, T.G. Dinan, G. Clarke, and J.F.
937 Cryan. 2023. Critical windows of early-life microbiota disruption on behaviour,
938 neuroimmune function, and neurodevelopment. *Brain Behav Immun* 108:309–
939 327.
940 Masuyama, H., T. Mitsui, E. Nobumoto, and Y. Hiramatsu. 2015. The Effects of High-Fat
941 Diet Exposure In Utero on the Obesogenic and Diabetogenic Traits Through
942 Epigenetic Changes in Adiponectin and Leptin Gene Expression for Multiple
943 Generations in Female Mice. *Endocrinology* 156:2482–2491.
944 Mattiola, I., A. Mantovani, and M. Locati. 2021. The tetraspan MS4A family in
945 homeostasis, immunity, and disease. *Trends Immunol* 42:764–781.
946 Minter, M.R., R. Hinterleitner, M. Meisel, C. Zhang, V. Leone, X. Zhang, P. Oyler-Castrillo,
947 X. Zhang, M.W. Musch, and X. Shen. 2017. Antibiotic-induced perturbations in
948 microbial diversity during post-natal development alters amyloid pathology in an
949 aged APPSWE/PS1ΔE9 murine model of Alzheimer's disease. *Scientific reports*
950 7:10411.
951 Minter, M.R., C. Zhang, V. Leone, D.L. Ringus, X. Zhang, P. Oyler-Castrillo, M.W. Musch, F.
952 Liao, J.F. Ward, and D.M. Holtzman. 2016. Antibiotic-induced perturbations in gut
953 microbial diversity influences neuro-inflammation and amyloidosis in a murine
954 model of Alzheimer's disease. *Scientific reports* 6:30028.
955 Paolicelli, R.C., A. Sierra, B. Stevens, M.-E. Tremblay, A. Aguzzi, B. Ajami, I. Amit, E.
956 Audinat, I. Bechmann, M. Bennett, F. Bennett, A. Bessis, K. Biber, S. Bilbo, M.
957 Blurton-Jones, E. Boddeke, D. Brites, B. Brône, G.C. Brown, O. Butovsky, M.J.

Carson, B. Castellano, M. Colonna, S.A. Cowley, C. Cunningham, D. Davalos, P.L. De Jager, B. de Strooper, A. Denes, B.J.L. Eggen, U. Eyo, E. Galea, S. Garel, F. Ginhoux, C.K. Glass, O. Gokce, D. Gomez-Nicola, B. González, S. Gordon, M.B. Graeber, A.D. Greenhalgh, P. Gressens, M. Greter, D.H. Gutmann, C. Haass, M.T. Heneka, F.L. Heppner, S. Hong, D.A. Hume, S. Jung, H. Kettenmann, J. Kipnis, R. Koyama, G. Lemke, M. Lynch, A. Majewska, M. Malcangio, T. Malm, R. Mancuso, T. Masuda, M. Matteoli, B.W. McColl, V.E. Miron, A.V. Molofsky, M. Monje, E. Mracsko, A. Nadjar, J.J. Neher, U. Neniskyte, H. Neumann, M. Noda, B. Peng, F. Peri, V.H. Perry, P.G. Popovich, C. Pridans, J. Priller, M. Prinz, D. Ragozzino, R.M. Ransohoff, M.W. Salter, A. Schaefer, D.P. Schafer, M. Schwartz, M. Simons, C.J. Smith, W.J. Streit, T.L. Tay, L.-H. Tsai, A. Verkhratsky, R. von Bernhardi, H. Wake, V. Wittamer, S.A. Wolf, L.-J. Wu, and T. Wyss-Coray. 2022. Microglia states and nomenclature: A field at its crossroads. *Neuron* 110:3458–3483.

Parums, D.V. 2024. A Review of the Current Status of Disease-Modifying Therapies and Prevention of Alzheimer's Disease. *Med Sci Monit* 30:e945091.

Price, D.L., and S.S. Sisodia. 1998. Mutant genes in familial Alzheimer's disease and transgenic models. *Annu Rev Neurosci* 21:479–505.

Radde, R., T. Bolmont, S.A. Kaeser, J. Coomaraswamy, D. Lindau, L. Stoltze, M.E. Calhoun, F. Jäggi, H. Wolburg, S. Gengler, C. Haass, B. Ghetti, C. Czech, C. Hölscher, P.M. Mathews, and M. Jucker. 2006. Abeta42-driven cerebral amyloidosis in transgenic mice reveals early and robust pathology. *EMBO Rep* 7:940–946.

Ruhl, D.A., E. Bomba-Warczak, E.T. Watson, M.M. Bradberry, T.A. Peterson, T. Basu, A. Frelka, C.S. Evans, J.S. Briguglio, T. Basta, M.H.B. Stowell, J.N. Savas, A. Roopra,

R.A. Pearce, R.C. Piper, and E.R. Chapman. 2019. Synaptotagmin 17 controls neurite outgrowth and synaptic physiology via distinct cellular pathways. *Nat Commun* 10:3532.

Saha, P., I.Q. Weigle, N. Slimmon, P.B. Poli, P. Patel, X. Zhang, Y. Cao, J. Michalkiewicz, A. Gomm, C. Zhang, R.E. Tanzi, N. Dylla, A. Al-Hendy, and S.S. Sisodia. 2024. Early modulation of the gut microbiome by female sex hormones alters amyloid pathology and microglial function. *Sci Rep* 14:1827.

Salia, S., F.F. Burke, M.E. Hinks, A.M. Randell, M.A. Matheson, S.G. Walling, and A. Swift-Gallant. 2025. Gut microbiota transfer from the preclinical maternal immune activation model of autism is sufficient to induce sex-specific alterations in immune response and behavioural outcomes. *Brain Behav Immun* 123:813–823.

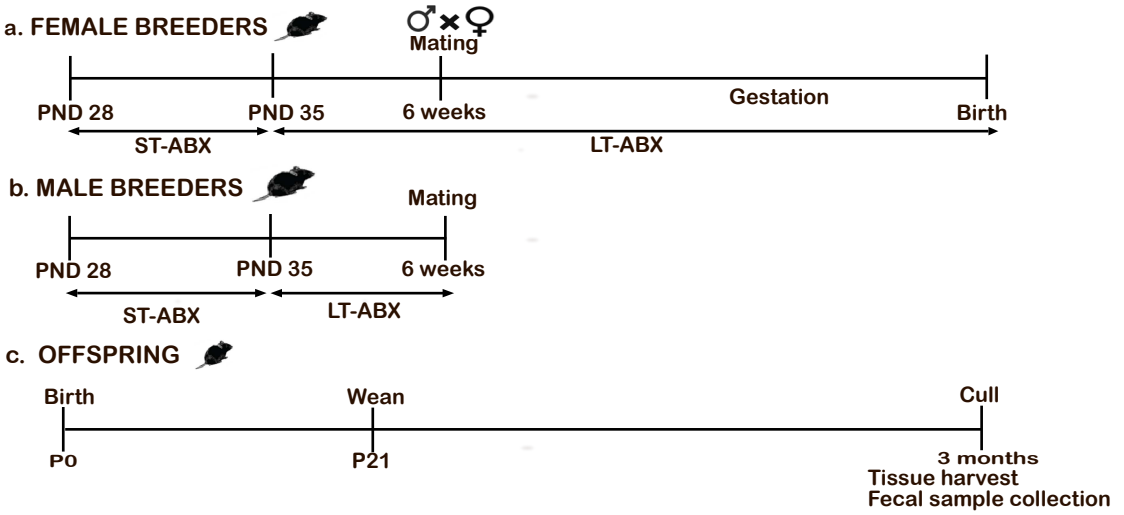
Thion, M.S., D. Low, A. Silvin, J. Chen, P. Grisel, J. Schulte-Schrepping, R. Blecher, T. Ulas, P. Squarzoni, G. Hoeffel, F. Coulpier, E. Siopi, F.S. David, C. Scholz, F. Shihui, J. Lum, A.A. Amoyo, A. Larbi, M. Poidinger, A. Buttgereit, P.M. Lledo, M. Greter, J.K.Y. Chan, I. Amit, M. Beyer, J.L. Schultze, A. Schlitzer, S. Pettersson, F. Ginhoux, and S. Garel. 2018. Microbiome Influences Prenatal and Adult Microglia in a Sex-Specific Manner. *Cell* 172:500–516 e516.

Vuong, H.E., G.N. Pronovost, D.W. Williams, E.J.L. Coley, E.L. Siegler, A. Qiu, M. Kazantsev, C.J. Wilson, T. Rendon, and E.Y. Hsiao. 2020. The maternal microbiome modulates fetal neurodevelopment in mice. *Nature* 586:281–286.

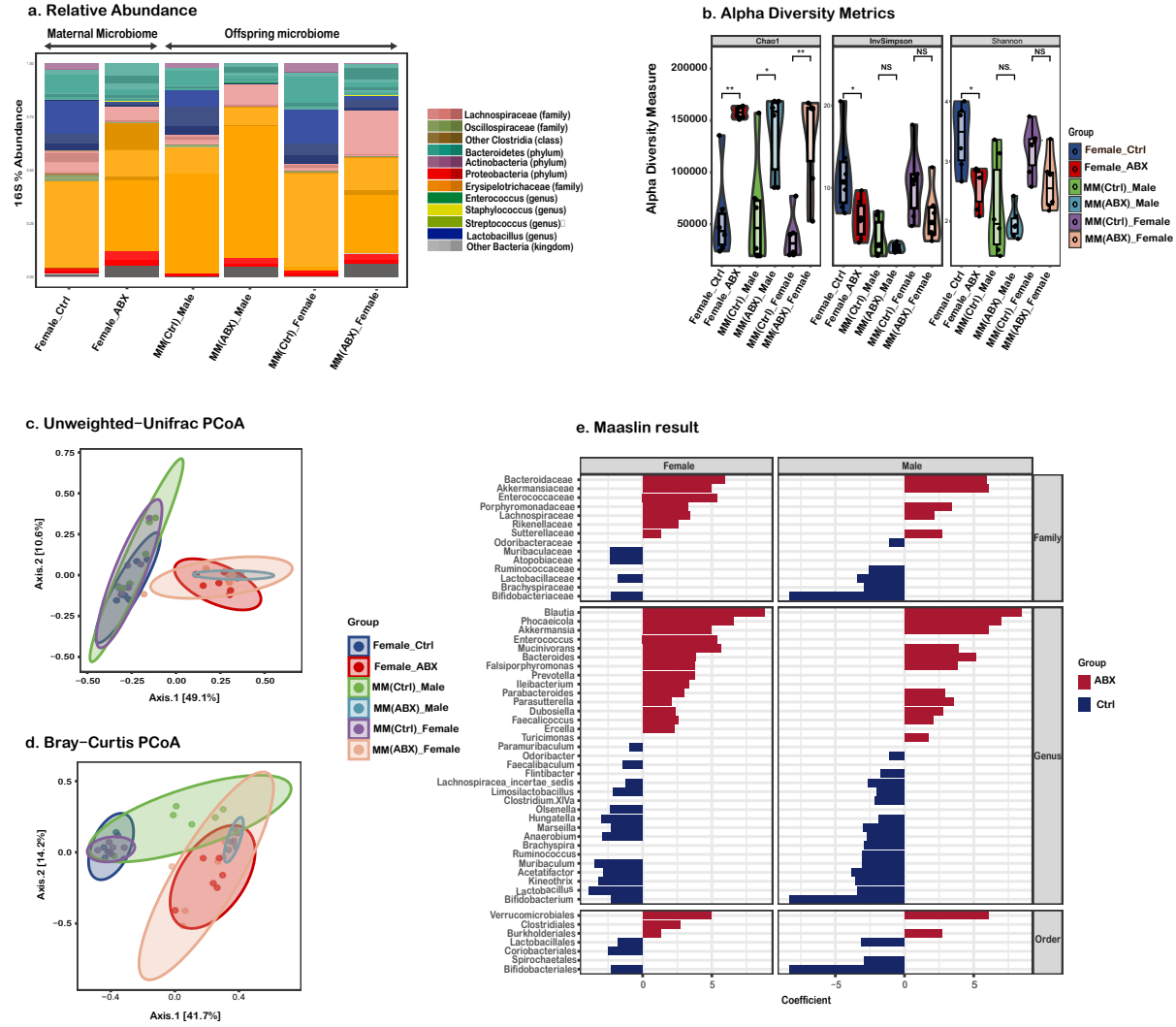
Xi, Y., Y. Zhang, Y. Zhou, Q. Liu, X. Chen, X. Liu, T. Grune, L. Shi, M. Hou, and Z. Liu. 2023. Effects of methionine intake on cognitive function in mild cognitive impairment patients and APP/PS1 Alzheimer's Disease model mice: Role of the cystathionine-beta-synthase/H(2)S pathway. *Redox Biol* 59:102595.

1006 Xing, Z., and B.P. Tu. 2025. Mechanisms and rationales of SAM homeostasis. *Trends in*
1007 *Biochemical Sciences* 50:242–254.
1008 Yan, C., B. He, C. Wang, W. Li, S. Tao, J. Chen, Y. Wang, L. Yang, Y. Wu, and Z. Wu. 2025.
1009 Methionine in embryonic development: metabolism, redox homeostasis,
1010 epigenetic modification and signaling pathway. *Critical Reviews in Food Science*
1011 *and Nutrition* 1–24.
1012 Young, C.E., and M.A. Samuel. 2025. Microglia sensing of peripheral signals that bridge
1013 the brain and body. *Mol Neurodegener* 20:114.
1014 Zhang, Y., Y. Wang, Y. Li, J. Pang, A. Höhn, W. Dong, R. Gao, Y. Liu, D. Wang, Y. She, R.
1015 Guo, and Z. Liu. 2024. Methionine restriction alleviates diabetes-associated
1016 cognitive impairment via activation of FGF21. *Redox Biology* 77:103390.
1017

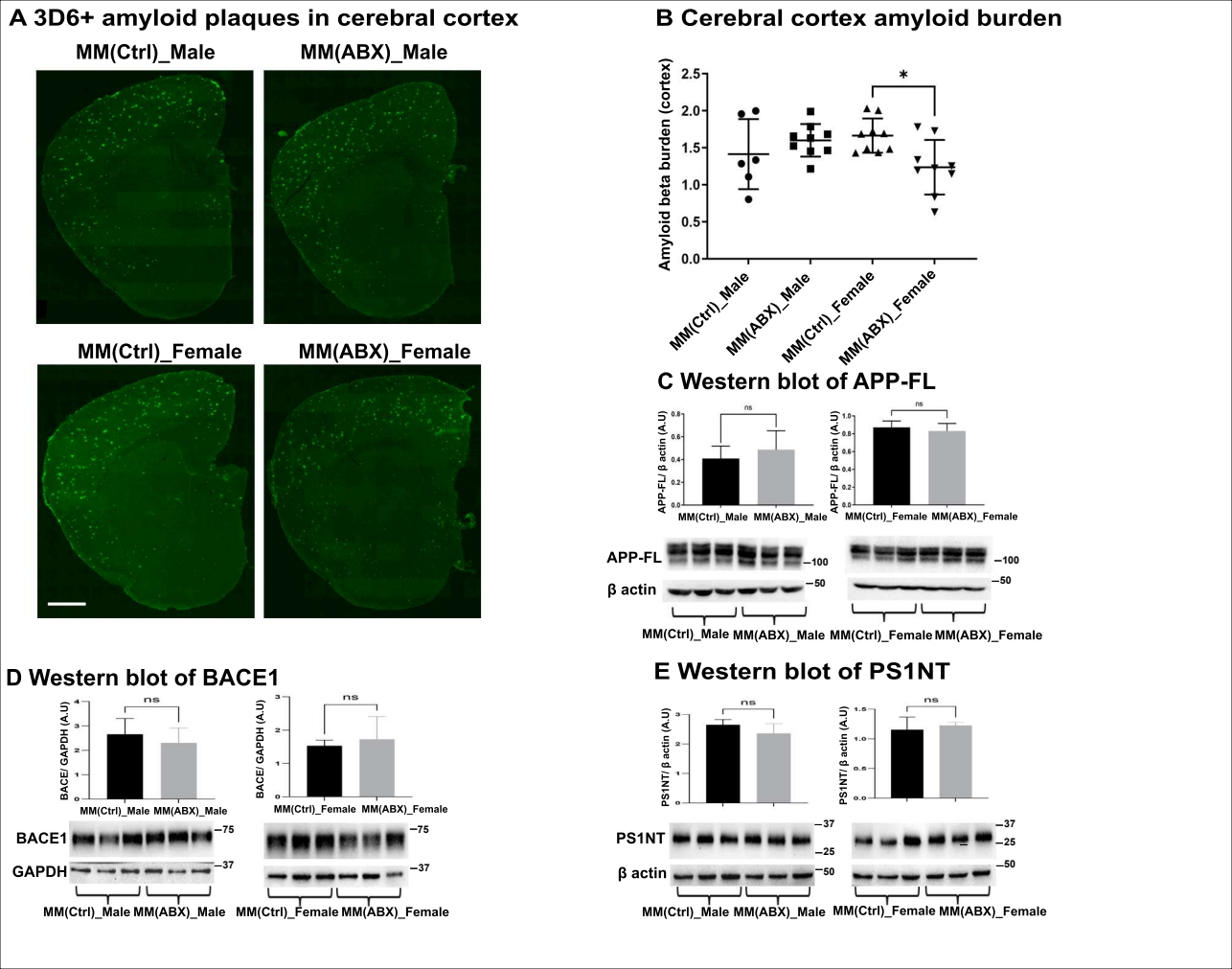
A Experimental Design



B 16srRNA sequencing analysis

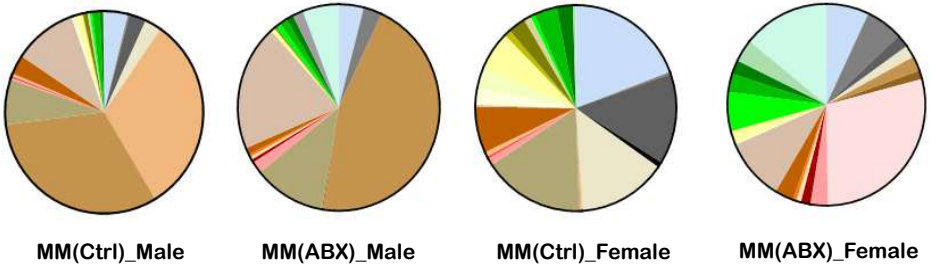


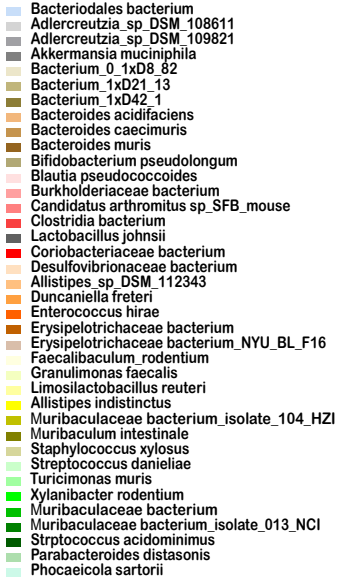
taxon


A 3D6+ amyloid plaques in cerebral cortex
MM(Ctrl)_Male
MM(ABX)_Male
MM(Ctrl)_Female
MM(ABX)_Female
B Cerebral cortex amyloid burden
Amyloid beta burden (cortex)
2.5
2.0
1.5
1.0
0.5
0.0
*
MM(Ctrl)_Male
MM(ABX)_Male
MM(Ctrl)_Female
MM(ABX)_Female
C Western blot of APP-FL
APP-FL/ β actin (A.U)
ns
MM(Ctrl)_Male
MM(ABX)_Male
MM(Ctrl)_Female
MM(ABX)_Female
APP-FL
β actin
100
50
D Western blot of BACE1
BACE/ GAPDH (A.U)
ns
MM(Ctrl)_Male
MM(ABX)_Male
MM(Ctrl)_Female
MM(ABX)_Female
BACE1
GAPDH
75
37
E Western blot of PS1NT
PS1NT/ β actin (A.U)
ns
PS1NT
β actin
37
25
50

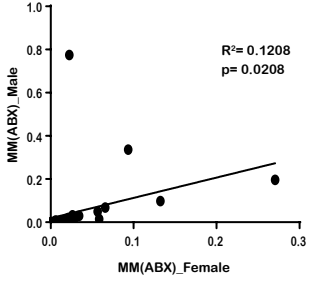
A Metagenomics analysis

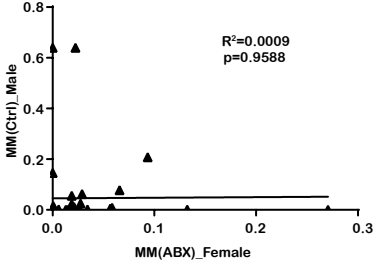
a Piechart showing species distrbution

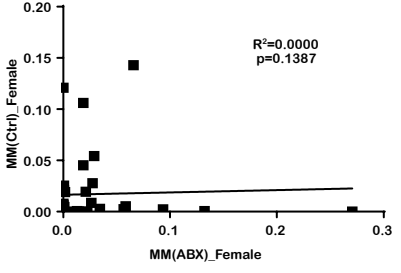




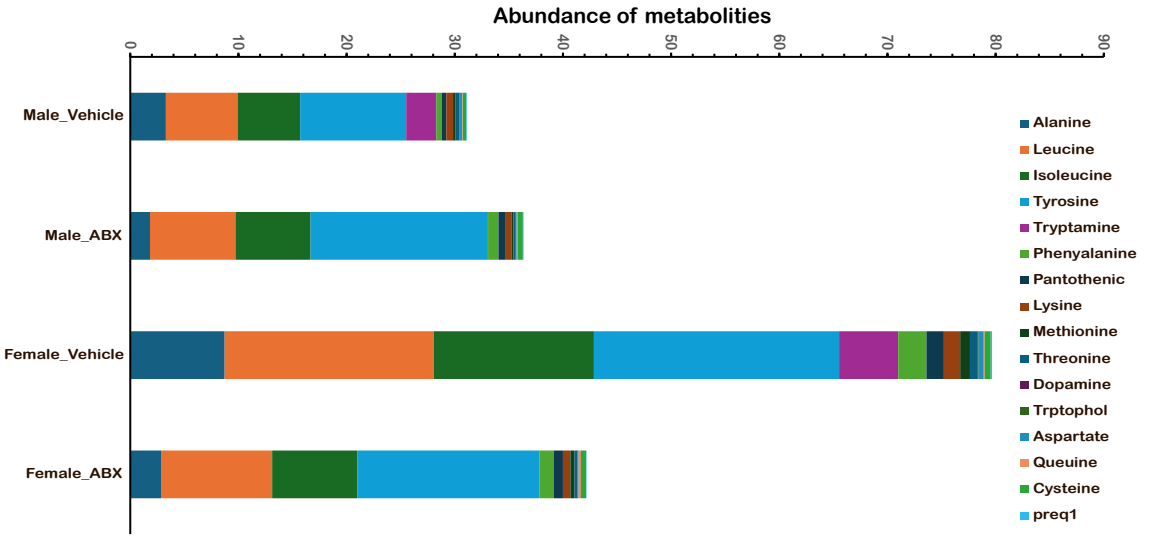
b Linear regression–based correlation analysis



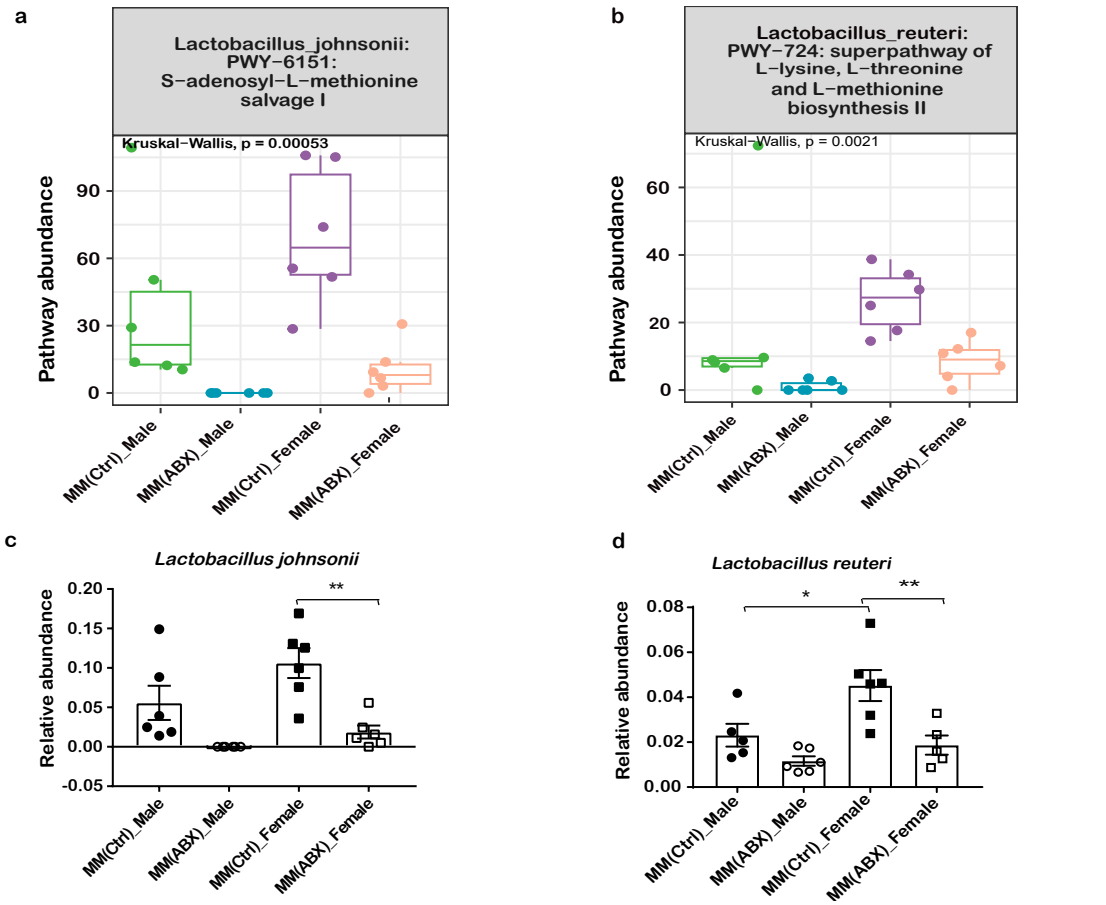




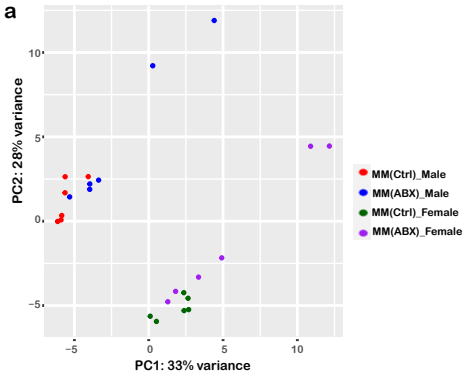
A Metabolomics analysis

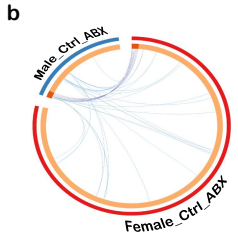


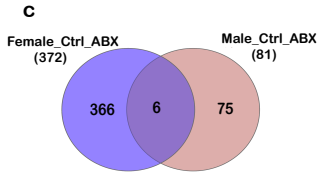
B Functional metagenomics analysis

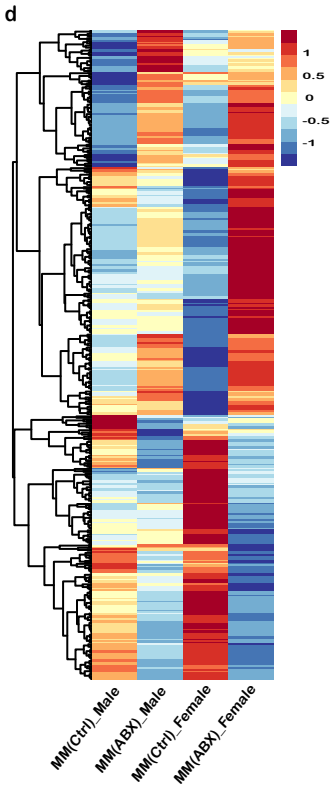


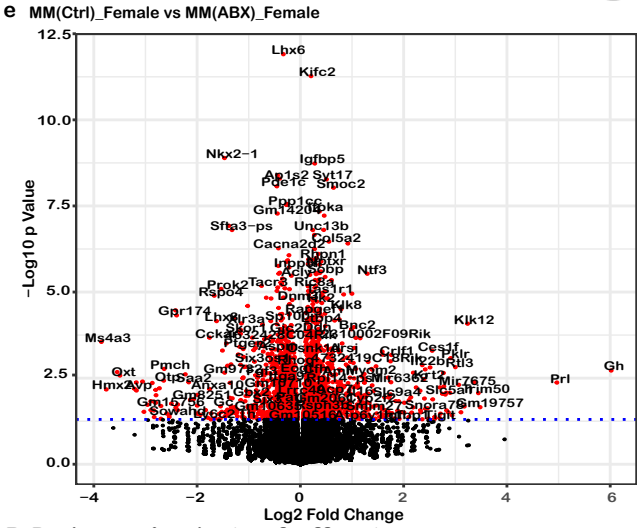
A Cortical RNA transcriptomics analysis of male and female offsprings





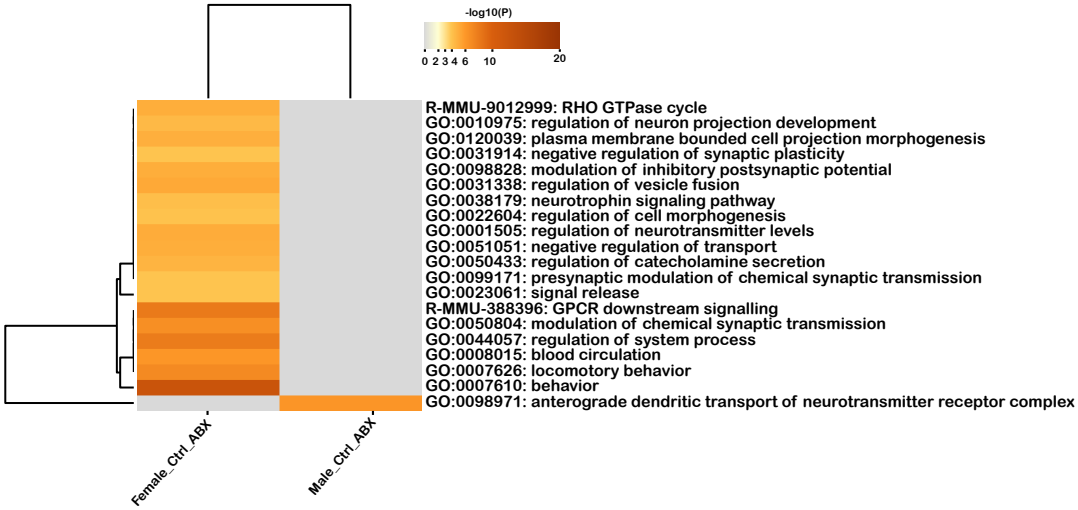




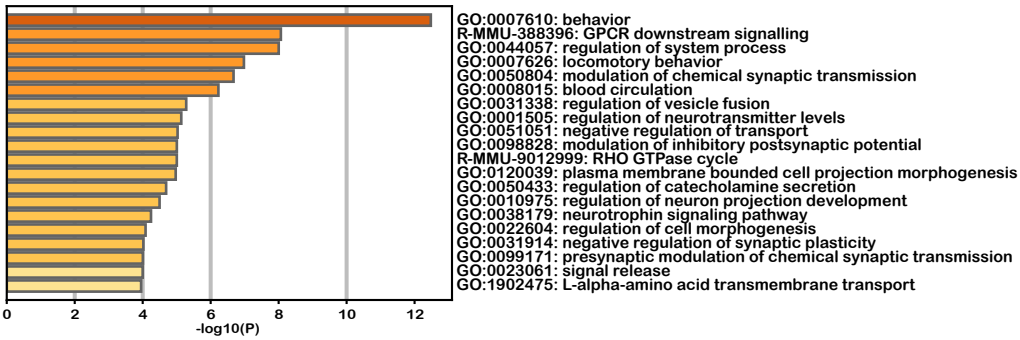


B Pathway Analysis of offsprings

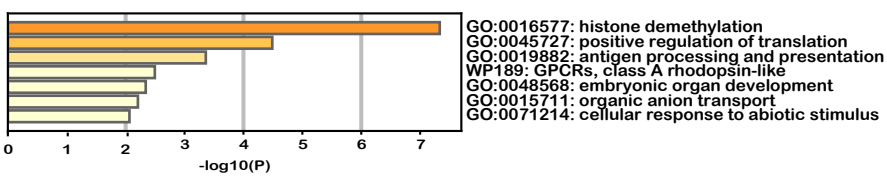
a MM (Ctrl vs ABX): Female vs Male

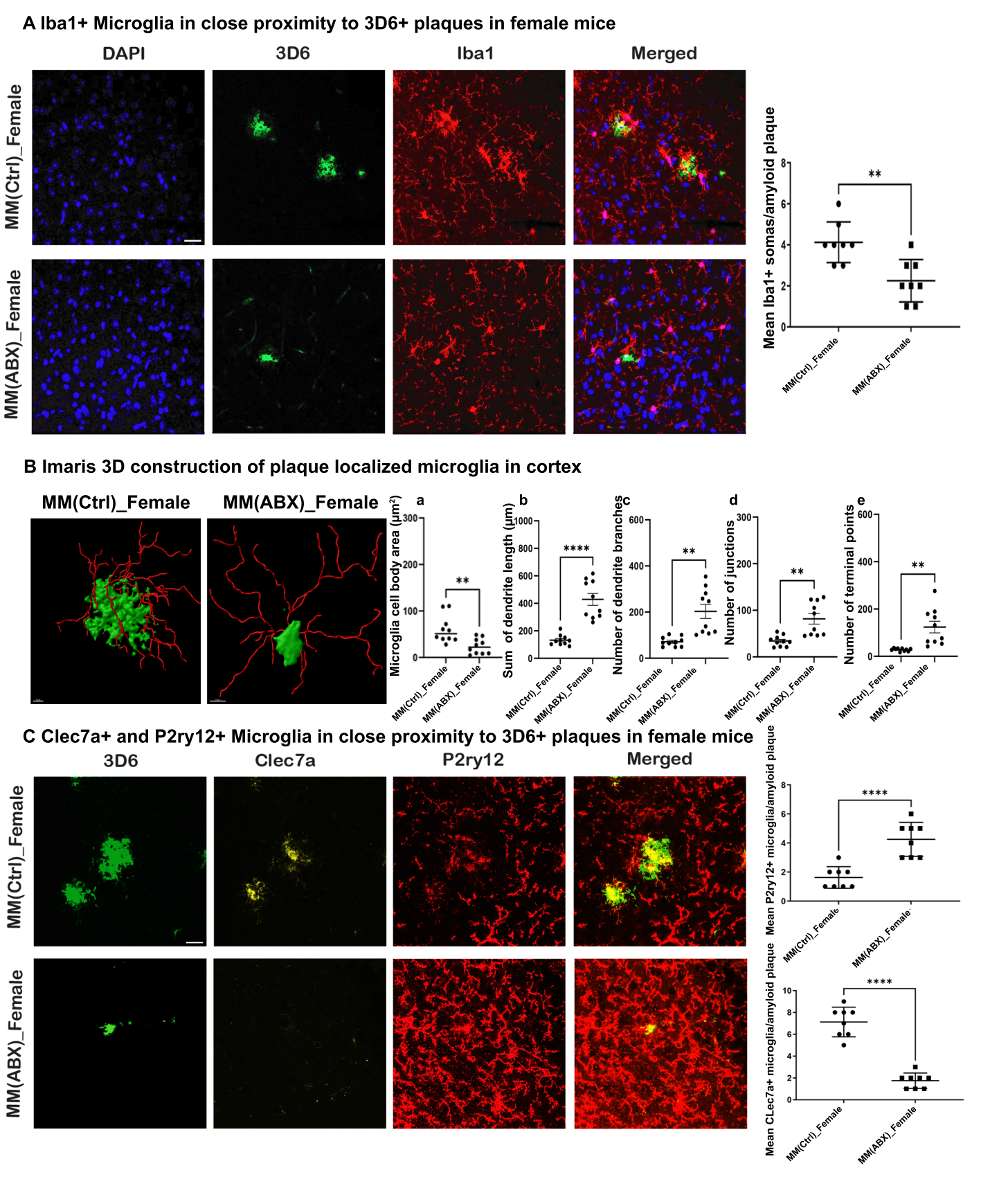


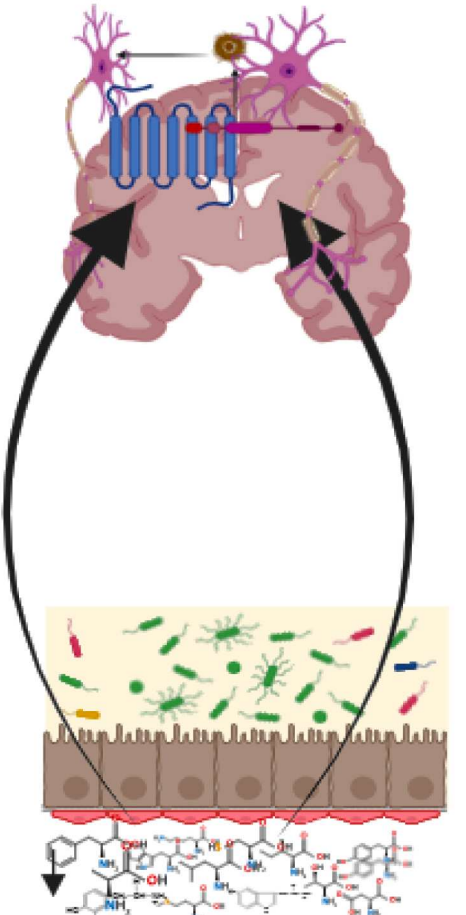
b MM(Ctrl)_Female vs MM(ABX)_Female



c MM(ABX)_Female vs MM(ABX)_Male




A Iba1+ Microglia in close proximity to 3D6+ plaques in female mice
DAPI
3D6
Iba1
Merged
MM(Ctrl)_Female
MM(ABX)_Female
Mean Iba1+ somas/amyloid plaque
**
MM(Ctrl)_Female
MM(ABX)_Female
B Imaris 3D construction of plaque localized microglia in cortex
MM(Ctrl)_Female
MM(ABX)_Female
a
Microglia cell body area (µm²)
**
b
Sum of dendrite length (µm)
****
c
Number of dendrite branches
**
d
Number of junctions
**
e
Number of terminal points
**
MM(Ctrl)_Female
MM(ABX)_Female
C Clec7a+ and P2ry12+ Microglia in close proximity to 3D6+ plaques in female mice
3D6
Clec7a
P2ry12
Merged
MM(Ctrl)_Female
MM(ABX)_Female
Mean P2ry12+ microglia/amyloid plaque
****
Mean CLec7a+ microglia/amyloid plaque
****
MM(Ctrl)_Female
MM(ABX)_Female



Supplementary Files

This is a list of supplementary files associated with this preprint. Click to download.

- Figure1S.pdf
- Figure2S.pdf
- Figure4S.pdf